

# CASHG: Context-Aware Stylized Online Handwriting Generation

Jinsu Shin, Sungeun Hong\*, and JinYeong Bak\*

Sungkyunkwan University, Suwon, Korea  
{jinsu0000, csehong, jy.bak}@skku.edu

Online handwriting represents strokes as time-ordered trajectories, which makes handwritten content easier to transform and reuse in a wide range of applications. However, generating natural *sentence-level* online handwriting that faithfully reflects a writer’s style remains challenging, since sentence synthesis demands context-dependent characters with stroke continuity and spacing. Prior methods treat these boundary properties as implicit outcomes of sequence modeling, which becomes unreliable at the sentence scale and under limited compositional diversity. We propose CASHG, a context-aware stylized online handwriting generator that explicitly models inter-character connectivity for style-consistent sentence-level trajectory synthesis. CASHG uses a *Character Context Encoder* to obtain character identity and sentence-dependent context memory and fuses them in a bigram-aware sliding-window Transformer decoder that emphasizes local predecessor–current transitions, complemented by *gated context fusion* for sentence-level context. Training proceeds through a three-stage curriculum from isolated glyphs to full sentences, improving robustness under sparse transition coverage. We further introduce *Connectivity and Spacing Metrics (CSM)*, a boundary-aware evaluation suite that quantifies cursive connectivity and spacing similarity. Under benchmark-matched evaluation protocols, CASHG consistently improves CSM over comparison methods while remaining competitive in DTW-based trajectory similarity, with gains corroborated by a human evaluation.<sup>1</sup>

**Keywords:** Online Handwriting · Sentence Generation · Inter-Character Connectivity · Spacing · Transformer

## 1 Introduction

Online handwriting represents pen motion as a time-ordered sequence of coordinates, making handwritten content easier to transform and reuse across a wide range of applications [9, 28]. Recent generative models [8, 12, 30] have shown strong performance across modalities, but *sentence-level online handwriting* generation with faithful writer-style reproduction remains challenging. Beyond plausible glyph shapes, realistic sentence-level handwriting must preserve *inter-character connectivity*—including kerning, word spacing, and cursive-like

\* Corresponding authors

<sup>1</sup> Code and Data: <https://github.com/jinsu0000/cashg-official>

**Table 1:** Property comparison of online handwriting generation methods.

Method	No Content Img. <sup>a</sup>	Word Spacing	Explicit Conn. <sup>b</sup>	Img. Style Ref. <sup>c</sup>
SDT [6]	No	No	No	Yes
DSD [20]	Yes	No	No	No
DeepWriting [1]	Yes	Part. <sup>d</sup>	No	No
OLHWG [33]	Yes	Yes	No	No
<b>CASHG (Ours)</b>	Yes	Yes	Yes	Yes

<sup>a</sup> No extra rendered content image is required beyond the style reference.

<sup>b</sup> The method explicitly models or supervises cursive like joins.

<sup>c</sup> The method can leverage an image based style reference.

<sup>d</sup> Part. indicates partial or implicit support.

	CASHG vs DSD [20]		CASHG vs DeepWriting [1]	
	Connectivity	Spacing	Connectivity	Spacing
Style Reference				
CASHG (Ours)				
Baselines				

**Fig. 1: Inter-character connectivity and spacing comparison.** Rows show style reference, CASHG, and the benchmark-matched comparison protocol. Columns compare connectivity and spacing under DSD and DeepWriting settings.

boundary transitions [1, 20, 33]. These local boundary dynamics shape the global writing flow; thus, even minor boundary artifacts (e.g., spacing or unintended stroke breaks) become salient in long sentences.

Existing sentence-level handwriting generation methods have pursued stylization through different input designs. To capture a writer’s style, prior work encodes writer information from sentence-level trajectory references or from global style descriptors from multiple reference samples [20]. Some approaches additionally rely on font-rendered content images to supply character identity cues for the target text [6]. These strategies can reproduce global appearance but often struggle to faithfully model boundary behavior at the sentence level. As summarized in Table 1, prior methods address parts of this design space, but none simultaneously support image-based style references, word-level spacing, and *explicit* inter-character connectivity modeling. As shown in Figure 1, baselines such as DSD [20] and DeepWriting [1] can produce unnatural kerning, missing or awkward cursive joins, and rigid word spacing even when individual glyphs look plausible. This limitation arises because prior methods treat boundary behavior as an implicit outcome of sequence modeling.

We propose CASHG, a **C**ontext-**A**ware **S**tylized **O**nline **H**andwriting **G**enerator for style-consistent sentence-level trajectory synthesis with explicit inter-character

connectivity modeling. CASHG addresses the limitations above through three complementary components. First, a *Character Context Encoder* produces two decoupled signals: a deterministic *Character-Identity Embedding* specifying which character to draw, and a position-dependent *context memory* modulating how it should appear and connect within the sentence. Second, a *bigram-aware sliding-window Transformer (Bi-SWT) decoder* explicitly models predecessor, current character transitions, directly supervising the local boundary dynamics that govern kerning and cursive joins. Bigram conditioning offers a principled trade-off: higher-order n-gram windows increase compositional sparsity under limited sentence data, whereas bigram windows retain the dominant local connectivity signal while enabling robust reuse of transition patterns across positions. Longer-range context is handled separately through *gated context fusion*, which adaptively blends sentence-level context memory into the decoding process without collapsing writer-specific stylization. Third, CASHG employs connectivity-aware supervision, explicit pen-state classification including a dedicated CURSIVEEOC label for pen-down character continuation, together with a Vertical Drift Loss that regularizes predecessor-current boundary alignment. We further adopt a three-stage curriculum (glyphs  $\rightarrow$  bigrams  $\rightarrow$  sentences) to improve training stability and composition coverage. [Figure 2](#) shows the overall architecture, and our experiments demonstrate strong sentence-level generation quality under benchmark-matched evaluation protocols.

To quantify boundary improvements beyond conventional trajectory metrics, we introduce *Connectivity and Spacing Metrics (CSM)*, a boundary-aware evaluation suite comprising cursive connectivity and spacing similarity metrics reported under writer-macro aggregation. Under benchmark-matched evaluation protocols, CASHG consistently improves CSM while remaining competitive in DTW-based trajectory similarity, findings corroborated by a human evaluation. Our contributions are summarized as follows:

- **Context-aware sentence-level trajectory synthesis.** We propose a context-fusion mechanism with per-character context memory and show context-dependent character realization in sentence-level trajectory synthesis.
- **Robust local connectivity modeling under sparse transition coverage.** We propose a bigram-aware sliding-window Transformer decoder and show robust predecessor–current transition modeling that improves *Inter-Character Connectivity* under sparse transition coverage.
- **Connectivity and Spacing Metrics (CSM) for boundary evaluation.** We introduce CSM for boundary-aware evaluation of *Inter-Character Connectivity* and spacing, including continuity ( $F1_{\text{Cursive}}$ , CRE) and spacing similarity (KGS, SSS) with writer-macro aggregation.

## 2 Related Work

### 2.1 Personalized Writer Stylization

Online handwriting records the pen motion as a time-ordered sequence of coordinates (trajectory), while offline handwriting is observed only as a static,

pixel-based image [9, 28]. A central goal of personalized online handwriting generation is to stylize a writer from a small set of reference samples while preserving the target text content. Previous work improves controllability by separating the writer-dependent style from character and glyph-related factors, using factorized conditions for writer-consistent character generation [6, 20, 35, 41]. These works establish a strong foundation for a style-conditioned personalized handwriting synthesis. Recent trajectory-based progress also includes *Elegantly Written* [23], which disentangles writer and character styles for online Chinese handwriting enhancement; while closely related in trajectory-based stylization, it targets character-level stroke-conditioned enhancement rather than our sentence-level generation setting. Style synthesis and disentanglement have also been explored in the offline image domain [11, 18, 25], further supporting the utility of factorized style and content conditioning, although these methods do not generate online trajectories. Despite practical challenges such as sensitivity to batch composition and dataset biases, metric- and contrastive-learning objectives have been widely adopted for stylization-oriented representation learning due to their strong ability to separate style-related embeddings [14, 15, 19].

CASHG leverages these principles and adapts them to sentence-level online handwriting generation. Specifically, CASHG achieves robust per-character stylization through disentangled writer/glyph style memories, and further fuses sentence context into this stylization via character-embedding-based context memory [5, 39], capturing context-dependent character variations as well as inter-character connectivity within trajectories.

## 2.2 Modeling Inter-Character Connectivity

A key property for sentence-level handwriting realism is *inter-character connectivity*—the boundary dynamics governing spacing (kerning) and stroke continuity (cursive joins) [21, 27, 31]. Many neural generators produce plausible character shapes, yet treat boundary behavior as an implicit outcome of sequence modeling [3, 13, 36, 37, 40], which can result in broken joins or unstable spacing in words and sentences. Prior handwriting generators such as DSD [20] and Deep-Writing [1] improve stylization and sequence generation, but do not explicitly supervise boundary-level connectivity as a primary training objective. Layout-oriented pipelines that decouple layout from glyph [33] explicitly model spacing and layout, but do not target stroke-level boundary continuation in online sentence generation.

Related evidence appears in adjacent tasks as well. ScrabbleGAN [10], GAN-Writing/HiGAN/SLOGAN [11, 18, 25], and trajectory-recovery methods [4, 26] can implicitly preserve inter-character connectivity through offline synthesis or trajectory recovery, but they differ in problem setting from online handwriting generation, where inter-character connectivity is modeled as a primary target. In contrast, CASHG explicitly models inter-character connectivity using boundary-aware pen states and character-conditioned context memory, enabling data-driven modeling of both spacing and cursive joins while preserving writer-consistent stylization.

### 2.3 Sentence-Level Generation under Limited Compositional Diversity

Sentence-level online handwriting generation is challenging in part because real sentence datasets [24] cover only a limited subset of the diverse character combinations and boundary contexts encountered at inference time. This data sparsity is especially problematic for boundary modeling: under-represented local character combinations can cause perceptually obvious failures even when isolated-character generation is strong.

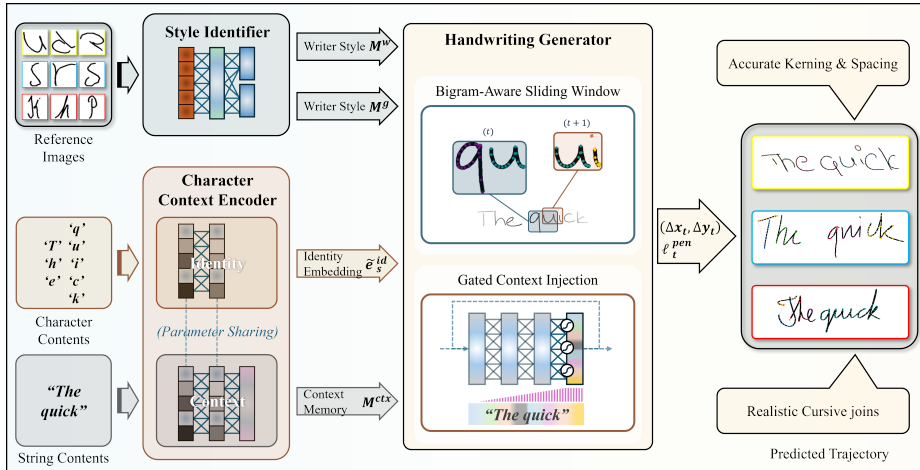
Earlier approaches rely primarily on RNN-family sequence models [13, 36, 37, 40]. DeepWriting [1] uses a conditional variational recurrent neural networks formulation for trajectory generation and editable digital ink, but long autoregressive generation can still suffer from drift and unstable local transitions. Transformer-based handwriting generators have also been explored [3], following broader sequence-modeling advances in Transformers [38], but explicit supervision of boundary-level connectivity remains limited. Layout-oriented pipelines [33] explicitly model spacing/layout, but do not directly target stroke-level boundary continuation for online sentence generation. While recent methods improve controllability through factorized stylization and conditioning [6, 41], robust sentence-level composition under limited transition diversity remains underexplored. CASHG addresses this gap with two complementary designs. First, we use curriculum learning from isolated glyphs to short character transitions and then full sentences, strengthening inter-character connectivity modeling before long-context composition. Second, we employ a bigram-aware sliding-window Transformer decoder that prioritizes local predecessor-conditioned synthesis, while integrating sentence-level context memory via a gated context-fusion mechanism. This design improves robustness to under-represented character combinations while still benefiting from sentence-conditioned context.

## 3 CASHG

CASHG targets sentence-level online handwriting generation with explicit *inter-character connectivity* modeling. CASHG stands for Context-Aware Stylized Online Handwriting Generation. It combines (i) a *Character Context Encoder* for context-aware conditioning, (ii) a *bigram-aware sliding-window Transformer decoder* for local transition modeling under limited coverage, and (iii) connectivity-aware supervision via pen state classification and boundary-level geometric regularization. CASHG further employs disentangled style and text-side conditioning, together with stage-wise training for stable optimization. Figure 2 shows the full pipeline. We use subscripts for sequence indices (e.g.,  $s, t$ ), superscripts for representation or type labels (e.g.,  $\text{id}, \text{ctx}, \text{sty}$ ), and roman subscripts for module names or semantic labels (e.g.,  $f_{\text{text}}, f_{\text{ctx}}$ ).

### 3.1 Character Context Encoder and Gated Context Fusion

The Character Context Encoder provides two signals for sentence-level generation. It produces a *Character-Identity Embedding* that specifies *which character*

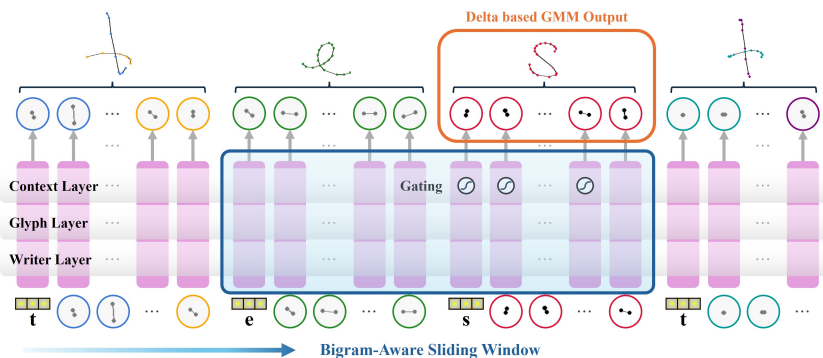


**Fig. 2: Overview of CASHG.** Reference handwriting images are encoded into *Writer-style memory*  $M^w$  and *Glyph-style memory*  $M^g$ . The *Character Context Encoder* is used in two input modes: isolated-character inputs produce deterministic *Character-Identity Embeddings*, while sentence inputs are further processed by a lightweight Transformer encoder to produce position-dependent *context memory*. The handwriting generator synthesizes trajectories with a bigram-aware sliding-window Transformer decoder and integrates context memory through *gated context fusion*, enabling writer-consistent glyph formation together with explicit inter-character connectivity modeling (spacing/kerning and cursive joins).

to draw and a position-dependent *context memory* that modulates *how it should appear and connect in sentence context*. Both use a shared multilingual text encoder  $f_{\text{text}}$  (e.g., CANINE [5] or ByT5 [39]), and the context branch adds a lightweight Transformer encoder for sentence-dependent variation. For a Unicode character  $u$ , we encode it in isolation to avoid contextual leakage and obtain a deterministic identity anchor  $\mathbf{e}^{\text{id}}(u) = f_{\text{id}}(f_{\text{text}}([u])) \in \mathbb{R}^D$ , where  $f_{\text{id}}(\cdot)$  is a pooling-and-projection head.

In practice,  $\mathbf{e}^{\text{id}}(u)$  is cached for unique codepoints within a mini-batch for efficient deterministic reuse. To sharpen discrete identity signals, we augment the Character-Identity Embedding as  $\tilde{\mathbf{e}}^{\text{id}}(u) = \mathbf{e}^{\text{id}}(u) + \alpha \mathbf{P}\phi(u)$ , with  $\alpha \in \mathbb{R}_+$ . Here  $\phi(u)$  is a learnable code embedding,  $\mathbf{P}$  is a projection matrix, and  $\alpha$  is a learnable scalar initialized to a small value.

This improves identity separability (e.g., case-sensitive distinctions) while keeping identity specification separate from sentence-dependent modulation. For a sentence-level character sequence  $\mathbf{u} = (u_1, \dots, u_S)$ , we compute sentence-aware context memory as  $\mathbf{H}^{\text{text}} = \mathbf{W}_h f_{\text{text}}(\mathbf{u})$  and  $\mathbf{M}^{\text{ctx}} = f_{\text{ctx}}(\text{TransEnc}_{\text{ctx}}(\mathbf{H}^{\text{text}}))$ , with  $f_{\text{ctx}}(\cdot)$  a projection head. The vector  $\mathbf{m}_s^{\text{ctx}}$  varies with neighboring characters and sentence position, making it suitable for modeling inter-character connectivity (e.g., spacing/kerning and cursive joins). Because context memory aids inter-character connectivity but can interfere with writer and glyph styl-



**Fig. 3: Bigram-aware sliding-window Transformer decoding with gated context fusion.** CASHG decodes each character from a predecessor–current local window and autoregressively predicts trajectory deltas (GMM-based). Writer-style and Glyph-style memories provide stylization cues, and sentence-level context memory is fused through a learnable gate to adapt generation to local context, improving inter-character connectivity (e.g., kerning and cursive joins).

ization when overused, we introduce a learnable token-wise *gated context fusion* module.

$$\mathbf{g}_t = \sigma\left(f_{\text{gate}}\left(\left[\mathbf{h}_t^{\text{sty}}; \mathbf{m}_{s(t)}^{\text{ctx}}\right]\right)\right), \quad \mathbf{h}_t = (1 - \mathbf{g}_t) \odot \mathbf{h}_t^{\text{sty}} + \mathbf{g}_t \odot \mathbf{m}_{s(t)}^{\text{ctx}}, \quad (1)$$

where  $\mathbf{g}_t \in (0, 1)^D$  and  $s(t)$  maps token  $t$  to its character position. CASHG thus uses  $\tilde{\mathbf{e}}^{\text{id}}(u_s)$  as a stable identity anchor and  $\mathbf{m}_s^{\text{ctx}}$  as a sentence-dependent modulation signal, enabling improved character legibility and inter-character connectivity realism.

### 3.2 Bigram-Aware Sliding-Window Transformer Decoder

CASHG uses a BIGRAM-AWARE SLIDING-WINDOW TRANSFORMER DECODER (Bi-SWT decoder) to prioritize local predecessor-conditioned synthesis. This design serves two goals: (i) stabilizing adjacent boundary behavior (e.g., kerning and cursive joins) and (ii) improving robustness when sentence data provides limited coverage of character combinations. We adopt predecessor–current bigram windows because the target phenomena are primarily boundary-local. Larger  $n$ -gram windows increase compositional sparsity and reduce coverage in real handwriting datasets, whereas bigram windows preserve dominant local connectivity cues while enabling better reuse of transition patterns across sentence positions. Longer-range sentence context is handled separately through *context memory* and *gated context fusion*.

For character position  $s$ , let  $\tilde{\mathbf{e}}_s^{\text{id}}$  be the augmented Character-Identity Embedding from Sec. 3.1, and let  $\mathbf{y}_{s,1:T_s}$  denote the trajectory-token sequence for the character at position  $s$ . During training with teacher forcing, we construct a

local window from the predecessor and current characters:

$$\mathbf{X}_s = [ \tilde{\mathbf{e}}_{s-1}^{\text{id}}, \mathbf{y}_{s-1,1:T_{s-1}}, \tilde{\mathbf{e}}_s^{\text{id}}, \mathbf{y}_{s,1:T_s} ] \in \mathbb{R}^{L_s \times D}, \quad (2)$$

where  $L_s = 2 + T_{s-1} + T_s$ . For  $s = 1$ , the window reduces to the current-character stream only. At inference time,  $\mathbf{y}_{s-1,\cdot}$  is replaced by the model prediction, while the Bi-SWT decoder autoregressively generates the current character trajectory. Within each local window, the Bi-SWT decoder applies causal self-attention with key-padding masks for variable-length trajectory tokens. To encode relative ordering inside the predecessor-current window, we apply RoPE [34] to query and key projections. Each decoder block conditions on two complementary sources: (i) *Writer-style memory* and *Glyph-style memory* (Sec. 3.3), and (ii) the position-specific *context memory* (Sec. 3.1). The style memories provide writer-consistent stylization cues, while context memory provides sentence-dependent modulation related to local neighborhood and position. Context memory is integrated through *gated context fusion* in Eq. (1), allowing local adaptation without collapsing writer/glyph stylization.

The decoder predicts point-to-point trajectory deltas autoregressively rather than absolute coordinates. For each valid step  $t$ , the decoder hidden state  $\mathbf{h}_t$  is mapped to an output head that predicts bivariate  $K$ -component GMM parameters over  $(\Delta x_t, \Delta y_t)$  and 4-way pen-state logits. We use  $K = 20$ , and the head outputs  $(\boldsymbol{\theta}_t^{\text{gmm}}, \boldsymbol{\theta}_t^{\text{pen}}) = f_{\text{out}}(\mathbf{h}_t)$ . We obtain valid mixture parameters using standard squashing functions (e.g., softmax for mixture weights, exponential for standard deviations, and tanh for correlations). The pen state predictions serve as input to explicit boundary-event supervision (Sec. 3.4).

### 3.3 Disentangled Style and Explicit Text-Side Conditioning

CASHG separates style conditioning from text-side conditioning. As shown in Figure 2, the style pathway provides writer-consistent stylization, while the text-side pathway is factorized into a Character-Identity Embedding and a separate sentence-context pathway (Sec. 3.1). This separation preserves character correctness while enabling explicit inter-character connectivity modeling.

Following SDT-style pipelines [6], we use a Transformer-based style encoder with a CNN front-end to extract disentangled *Writer-style memory* and *Glyph-style memory* from reference handwriting images. The Writer-style memory captures global writer traits, whereas the Glyph-style memory captures character-dependent stylistic variation. These style memories are injected into the decoder via cross-attention for writer-consistent stylization. A CNN front-end (e.g., ResNet) is well suited to reference glyph images, which are single-channel grayscale patches with relatively small spatial resolution.

CASHG does not rely on image-based text-side inputs for character identity; instead, it uses a Character-Identity Embedding derived from Unicode codepoint inputs together with a separate sentence-context pathway. This eliminates the need for content image sets or font-rendered templates at inference time, reducing deployment overhead and improving input flexibility.

### 3.4 Training Objectives and Connectivity-Aware Supervision

We adopt a three-stage curriculum (glyph  $\rightarrow$  bigram  $\rightarrow$  sentence) to stabilize optimization under limited compositional diversity in sentence-level data, while keeping a shared objective form across stages. At stage  $k$ , the active generation loss is

$$\mathcal{L}_{\text{gen}}^{(k)} = \lambda_{\text{char}}^{(k)} \mathcal{L}_{\text{char}} + \lambda_{\text{bi}}^{(k)} \mathcal{L}_{\text{bi}} + \lambda_{\text{sent}}^{(k)} \mathcal{L}_{\text{sent}}, \quad (3)$$

where the three terms correspond to representative glyph samples, predecessor-current bigram windows, and sentence sliding windows, respectively. Using the decoder outputs, we optimize a masked GMM negative log-likelihood on valid trajectory steps:

$$\mathcal{L}_{\text{mdn}} = -\frac{1}{|\mathcal{V}|} \sum_{t \in \mathcal{V}} \log \left( \sum_{k=1}^K \pi_{t,k} \mathcal{N}_2(\Delta \mathbf{y}_t; \boldsymbol{\mu}_{t,k}, \boldsymbol{\Sigma}_{t,k}) \right), \quad (4)$$

where  $\mathcal{V}$  is the set of valid (non-padded) steps,  $\Delta \mathbf{y}_t = (\Delta x_t, \Delta y_t)$ , and  $\pi_{t,k}$  are mixture weights. We also apply masked cross-entropy on 4-way pen states (PM, PU, CURSIVEEOC, EOC) as  $\mathcal{L}_{\text{pen}} = -\frac{1}{|\mathcal{V}|} \sum_{t \in \mathcal{V}} \log p_{t, y_t^{\text{pen}}}^{\text{pen}}$ , where CURSIVEEOC explicitly supervises pen-down continuation across character boundaries (cursive joins). All pen state labels, including CURSIVEEOC, are deterministically derived from the preprocessed trajectory stream and boundary annotations. To preserve a unified trajectory formulation, we retain inter-word spaces as short pseudo-trajectory segments rather than dropping them.

For the bigram stream, we add a lightweight *Vertical Drift Loss (VDL)* as an auxiliary regularizer to reduce predecessor-current boundary misalignment, especially *y-drift* and effective *height-drift*. VDL penalizes mismatches in predecessor $\rightarrow$ current vertical offsets measured at three summary statistics (centroid, top band, bottom band):

$$\mathcal{L}_{\text{vdl}} = \frac{1}{|\mathcal{B}|} \sum_{b \in \mathcal{B}} \left( w_{\text{cen}} \|\hat{\delta}_b^{\text{cen}} - \delta_b^{\text{cen}}\|_2^2 + w_{\text{top}} \|\hat{\delta}_b^{\text{top}} - \delta_b^{\text{top}}\|_2^2 + w_{\text{bot}} \|\hat{\delta}_b^{\text{bot}} - \delta_b^{\text{bot}}\|_2^2 \right), \quad (5)$$

where  $\mathcal{B}$  is the set of valid bigram boundaries. VDL is computed in the same normalized trajectory coordinate system for predictions and ground truth and is used with a small coefficient (implementation details in the supplementary material). The total objective is  $\mathcal{L}_{\text{total}} = \mathcal{L}_{\text{gen}}^{(k)} + \lambda_{\text{style}} \mathcal{L}_{\text{style}}$ . We define the sequence loss as  $\mathcal{L}_{\text{seq}} = \mathcal{L}_{\text{mdn}} + \lambda_{\text{pen}} \mathcal{L}_{\text{pen}}$ . For the bigram stream, we add the vertical drift regularizer and use  $\mathcal{L}_{\text{bi}} = \mathcal{L}_{\text{seq}} + \lambda_{\text{vdl}} \mathcal{L}_{\text{vdl}}$ . We use  $\mathcal{L}_{\text{seq}}$  for both glyph and sentence streams.

## 4 Experiments

We evaluate CASHG on both sentence-level and glyph-level *online handwriting* generation. Since sentence realism depends on *inter-character connectivity* (kerning, word spacing, and cursive-like boundary joins) beyond glyph shape,

we report *Connectivity and Spacing Metrics* (CSM) as the primary boundary-aware suite ( $F1_{\text{Cursive}}$ , CRE, KGS, SSS), and additionally report *Dynamic Time Warping* (DTW) for global trajectory geometry. See the supplementary material for CSM details.

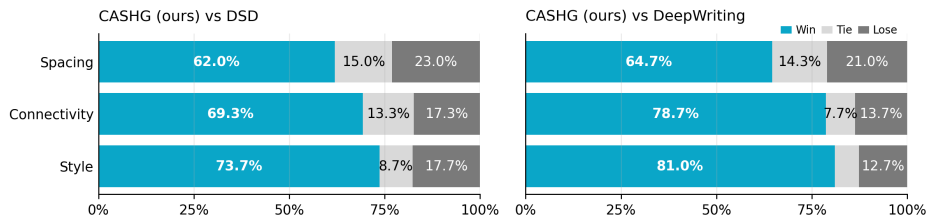
#### 4.1 Experimental Setup

A single unified comparison across all baselines is impractical and can be unfair because prior methods are defined under different input and output conventions. They differ in required inputs and style references, trajectory conventions, and benchmark protocols. For example, DSD [20] uses writer-dependent global style descriptors from multiple reference samples, while DeepWriting [1] conditions on sequential sentence-level trajectories. In the DeepWriting [1] benchmark, the evaluation data extends IAM with additional samples and we observed that some added samples have atypical aspect ratios. Enforcing a single normalization across such settings can shift the intended data distribution and unfairly affect methods tuned to the original benchmark conventions. We therefore conduct *benchmark-specific pairwise comparisons*. For each baseline, we retrain CASHG under the corresponding benchmark setting using the same train/test split or the benchmark-defined protocol. We apply identical preprocessing and metric implementation for both methods. Unless otherwise noted, all quantitative results use *fully autoregressive* inference with no teacher forcing at test time. We generate a single output sample per test input and compute DTW and CSM on that output. Results are shown side-by-side for coverage and should be interpreted within each benchmark protocol. For each protocol, metrics are computed per generated sentence and aggregated with writer-macro averaging with equal weight per writer.

**Language and granularity matched evaluation.** For sentence-level realism, we use English protocols where cursive joins and whitespace runs are prevalent. This makes joins, kerning, and spacing salient for CSM. As an additional evaluation of *glyph-level stylization*, we report character-level results on both English and Chinese protocols with large inventories and visually complex shapes. For glyph-level evaluation, we use the SDT-compatible protocol on CASIA-OLHWDB (1.0–1.2) for Chinese [11] and the corresponding English SDT benchmark. For sentence-level evaluation, we use CASIA-OLHWDB (2.0–2.2) under the OLHWG-compatible protocol [22, 33].

**Training data for qualitative examples and ablation.** For qualitative examples, human evaluation, and ablation, we construct a merged English sentence dataset from IAM [24] and BRUSH [20] to increase bigram diversity for the Bi-SWT decoder. IAM and BRUSH use different coordinate systems and point densities. We harmonize them via resampling to match point density while avoiding style loss from trajectory simplification. We then apply aspect-ratio-preserving height normalization ( $h = 1.0$ ). We also review character segmentation and fix inconsistencies following [17].

**Benchmark-matched sentence-level comparisons.** For sentence-level comparisons, CASHG is retrained under each benchmark-matched protocol. We



**Fig. 4:** Human evaluation of perceptual similarity in style, connectivity, and spacing under two comparison protocols (DSD, DeepWriting). Tie denotes *Cannot judge*.

use BRUSH for the DSD-style comparison, IAM-expanded for the DeepWriting comparison, and CASIA-OLHWDB (2.0–2.2) for the OLHWG comparison. We note DiffInk [29] as a relevant Chinese baseline but omit it from our comparisons due to the absence of publicly available code or checkpoints at the time of submission. For the BRUSH and DSD-style evaluation, we use a writer-disjoint split (150 train and 20 test writers) and disable RDP [7, 32] simplification during evaluation.

**Metrics and normalization.** We interpret DTW and CSM as complementary. We compute DTW [2] using Euclidean pointwise distance on  $(x, y)$  trajectories. We report  $DTW_{\text{raw}}$  and  $DTW_{\text{norm}} = DTW_{\text{raw}} / |GT|$ . Both prediction and GT are independently normalized by translation and height without rotation normalization. This can de-emphasize *inter-character connectivity* cues, so we also report CSM. We report CSM sub-scores (higher is better) including  $F1_{\text{Cursive}}$ , **CRE**, **KGS**, and **SSS**. They evaluate CURSIVEEOC boundary correctness and rate, and inter-character kerning and word spacing similarity (see the supplementary material). Undefined CSM terms are reported as - when there are no positive CURSIVEEOC boundaries or no whitespace runs. For baselines that output delta trajectories, we convert them to absolute coordinates and apply the same normalization before DTW and CSM computation.

## 4.2 Qualitative Comparison

We qualitatively evaluate CASHG from two complementary perspectives: (i) *model comparison* under benchmark-specific settings and (ii) *writer-style diversity* under fixed content.

**Human evaluation.** We conduct a blind A/B preference study with 30 participants. Each participant completes 20 trials in random order with 10 trials per protocol. In each trial, participants are given real writer reference samples and two candidates for the same sentence. They choose the closer one in terms of **Style**, **Inter-character connectivity**, and **Spacing**, with a *Cannot judge* option. Overall, CASHG is preferred under both protocols. Under DSD, CASHG wins 615 of 789 valid judgments and 111 judgments are *Cannot judge*. Under DeepWriting, CASHG wins 673 of 815 valid judgments and 85 judgments are *Cannot judge*. The criterion-wise breakdown is summarized in Figure 4.

		English				
GT	CHARACTERS	Trelawny	outrageous	succinct	Zeitgeist	payable
DSD	CHARACTERS	Trelawny	outrageous	succinct	Zeitgeist's	payable
CASHG(ours)	CHARACTERS	Trelawny	outrageous	succinct	Zeitgeist	payable
		Chinese				
GT		基于法律系要事	光各合客逐	赶给做锡斯饼魁鲜		
OLHWG		基于法律系要事	光各合客逐	赶给做锡斯饼魁鲜		
CASHG(ours)		基于法律系要事	光各合客逐	赶给做锡斯饼魁鲜		

**Fig. 5: Qualitative sentence-level comparison on BRUSH (English) and CASIA (Chinese).** English examples use BRUSH ground truth and are sampled from the corresponding subset of our merged IAM and BRUSH dataset. Compared with DSD and OLHWG, CASHG better preserves writer-consistent glyph shape and sentence-level structure, including local connectivity and spacing patterns.

Jackdaws love my big sphinx of quartz	你的笑容好暖熟悉,我一直想不起
Jackdaws love my big sphinx of quartz	你的笑容好暖熟悉,我一直想不起
Jackdaws love my big sphinx of quartz	你的笑容好暖熟悉,我一直想不起
Jackdaws love my big sphinx of quartz	你的笑容好暖熟悉,我一直想不起

**Fig. 6: Writer-style diversity under fixed content.** For the same sentence, CASHG produces distinct outputs conditioned on different writer-style references

Figure 5 compares CASHG against the corresponding baselines in the English and Chinese settings. English examples use ground truth trajectories from the BRUSH subset of our merged IAM and BRUSH dataset. In English, CASHG more faithfully reproduces writer-specific inter-character connectivity, including kerning, cursive-like joins, and word spacing, while preserving sentence-level flow. In contrast, baseline outputs more often show degraded inter-character connectivity or less consistent spacing patterns. On CASIA (Chinese), where explicit whitespace and cursive-like joining are less prominent, CASHG better preserves writer-specific glyph style and sentence-level visual consistency, especially for complex characters. Figure 6 shows *style diversity under fixed content*. For the same input sentence, CASHG generates distinct outputs conditioned on different writer-style references.

### 4.3 Glyph-Level Quantitative Results

We compare CASHG with SDT [6] on CASIA\_ENGLISH under a matched glyph-level protocol. We do not include a direct comparison with *Elegantly Written* [23], as it targets stroke-conditioned handwriting beautification/style transfer from an observed trace rather than CASHG’s fully data-driven generation setting. Table 2 shows that CASHG achieves

**Table 2:** Character-level DTW (lower-is-better) on SDT benchmarks

Method	English	Chinese
	DTW ↓	DTW ↓
Drawing [40]	1.8519	1.1813
DeepImitator [41]	1.6460	1.0622
WriteLikeYou-v2 [35]	1.6215	0.9289
SDT [6]	1.6048	0.8789
CASHG (ours)	<b>1.3649</b>	<b>0.8718</b>

a lower normalized and raw DTW as well as a lower standard deviation of normalized DTW, indicating a more accurate and more stable glyph trajectory generation. Although CASHG is designed for sentence-level generation, curriculum learning also improves the robustness of representative glyph generation. Because independent normalization de-emphasizes layout and boundary behavior, we next evaluate sentence-level generation with DTW and CSM.

### 4.4 Sentence-Level Quantitative Results

We evaluate sentence-level *online handwriting* generation using benchmark specific pairwise comparisons. Table 3 reports sentence-level results under matched protocols. Std. denotes the standard deviation of  $DTW_{norm}$  over sentences with writer-macro aggregation. For the OLHWG Chinese protocol, only **KGS** is reported because **F1<sub>Cursive</sub>/CRE** and **SSS** are not meaningful in this dataset (no cursive positives and no whitespace runs). Across DSD and DeepWriting, CASHG consistently improves CSM, indicating more faithful inter-character connectivity.  $DTW_{norm}$  also decreases with reduced variance (Std.), suggesting a more stable sentence-level decoding. In the DeepWriting comparison, we follow the benchmark protocol and symmetrically exclude outliers with segment errors in three or more characters for both models. Results show that CASHG not only preserves character shape and global layout fidelity, but also more faithfully reproduces inter-character connectivity and spacing patterns.

### 4.5 Ablation Study

We perform a  $2 \times 2$  ablation on the merged English sentence setting (IAM+BRUSH) to assess the contributions of the *Bi-SWT decoder* and *gated context fusion*. Table 4 reports DTW and CSM on the same validation subset under the same training schedule.

The full model achieves the best overall balance across DTW and CSM. Removing the Bi-SWT decoder degrades DTW and boundary-sensitive CSM metrics, indicating the importance of predecessor-conditioned local decoding for *inter-character connectivity*. Removing gated context fusion preserves part of the DTW gains but reduces CSM (especially  $F1_{Cursive}$  and KGS), showing that contextual modulation complements local bigram modeling.

**Table 3:** Sentence-level Connectivity and Spacing Metrics (CSM, higher-is-better) and DTW (lower-is-better) on pairwise-compatible comparison sets.

Benchmark <sup>a</sup>	Method	CSM ( $\uparrow$ )				DTW ( $\downarrow$ )		
		F1 <sub>Cursive</sub>	CRE	KGS	SSS	DTW <sub>norm</sub>	DTW <sub>raw</sub>	Std.
DSD [20]	Baseline	0.07	0.84	0.39	0.49	1.25	355.92	3.55
	CASHG (Ours)	<b>0.45</b>	<b>0.90</b>	<b>0.44</b>	<b>0.63</b>	<b>0.99</b>	<b>184.31</b>	<b>0.96</b>
DeepWriting [1]	Baseline	0.26	0.81	0.15	0.57	2.70	476.92	1.55
	CASHG (Ours)	<b>0.33</b>	<b>0.84</b>	<b>0.41</b>	<b>0.61</b>	<b>1.41</b>	<b>234.30</b>	<b>0.91</b>
OLHWG [33]	Baseline	- <sup>b</sup>	-	0.34	-	0.17	183.14	<b>0.02</b>
	CASHG (Ours)	- <sup>b</sup>	-	<b>0.40</b>	-	<b>0.14</b>	<b>166.14</b>	<b>0.02</b>

<sup>a</sup> English: DSD, DeepWriting, Chinese: OLHWG.<sup>b</sup> OLHWG: F1<sub>Cursive</sub>/CRE/SSS undefined (no cursive positives; no whitespace).**Table 4:** 2×2 ablation of the Bi-SWT decoder and gated context fusion.

Factors		CSM ( $\uparrow$ )				DTW ( $\downarrow$ )	
Bi-SWT	Ctx. Fusion	F1 <sub>Cursive</sub>	CRE	KGS	SSS	DTW <sub>norm</sub>	DTW <sub>raw</sub>
On	On	<b>0.49</b>	<b>0.91</b>	<b>0.49</b>	<b>0.71</b>	<b>0.51</b>	<b>169.87</b>
Off	On	0.37	0.88	0.44	0.40	0.60	186.90
On	Off	0.35	0.91	0.48	0.69	0.55	174.34
Off	Off	0.22	0.85	0.29	0.66	0.57	187.58

## 5 Conclusion

We presented CASHG, a context-aware stylized *online handwriting* generator for sentence-level trajectory synthesis. Realistic sentence-level handwriting requires modeling not only character shape but also *inter-character connectivity*, including kerning, spacing, and cursive-like boundary behavior. To address this, CASHG combines disentangled style conditioning with context-aware decoding and curriculum training from glyph-shape modeling to sentence-level generation. We also introduced *Connectivity and Spacing Metrics (CSM)*, which explicitly quantify sentence-level connectivity and spacing properties such as cursive boundary correctness and rate, kerning similarity, and word-spacing similarity. Across benchmark-specific pairwise comparisons, CASHG consistently improves connectivity and spacing fidelity under CSM while remaining competitive in DTW-based trajectory similarity, which is also reflected in human preference results on connectivity and spacing. Our ablations further confirm that both the Bi-SWT decoder and gated context fusion contribute to sentence realism and that the full model provides the best overall balance. Finally, this work highlights the need for standardized sentence-level protocols and metrics in online handwriting generation because existing methods differ in inputs, representations, and evaluation conventions. As future work, we will extend CASHG to broader scripts, improve robustness under scarce or mismatched style references, and encourage more standardized benchmarks and evaluation practices.

## References

1. Aksan, E., Pece, F., Hilliges, O.: Deepwriting: Making digital ink editable via deep generative modeling. In: CHI. pp. 1–14 (2018) [2](#), [4](#), [5](#), [10](#), [14](#), [32](#), [33](#), [34](#), [35](#), [41](#)
2. Berndt, D.J., Clifford, J.: Using dynamic time warping to find patterns in time series. In: KDD Workshop. pp. 359–370 (1994) [11](#), [31](#), [32](#), [39](#), [41](#)
3. Bhunia, A.K., Khan, S., Cholakkal, H., Anwer, R.M., Khan, F., Shah, M.: Handwriting transformers. In: ICCV. pp. 1066–1074. IEEE (2021) [4](#), [5](#)
4. Bhunia, A.K., Bhowmick, A., Bhunia, A.K., Konwer, A., Banerjee, P., Roy, P.P., Pal, U.: Handwriting trajectory recovery using end-to-end deep encoder-decoder network. In: ICPR. pp. 3639–3644. IEEE (2018) [4](#)
5. Clark, J.H., Garrette, D., Turc, I., Wieting, J.: Canine: Pre-training an efficient tokenization-free encoder for language representation. *TACL* **10**, 73–91 (2022) [4](#), [6](#), [27](#)
6. Dai, G., Zhang, Y., Wang, Q., Du, Q., Yu, Z., Liu, Z., Huang, S.: Disentangling writer and character styles for handwriting generation. In: CVPR. pp. 5977–5986 (2023) [2](#), [4](#), [5](#), [8](#), [13](#), [27](#)
7. Douglas, D.H., Peucker, T.K.: Algorithms for the reduction of the number of points required to represent a digitized line or its caricature. *Cartographica* **10**(2), 112–122 (1973) [11](#), [25](#), [26](#)
8. Esser, P., Kulal, S., Blattmann, A., Entezari, R., Müller, J., Saini, H., Levi, Y., Lorenz, D., Sauer, A., Boesel, F., et al.: Scaling rectified flow transformers for high-resolution image synthesis. In: ICML. pp. 12606–12633. PMLR (2024) [1](#)
9. Faundez-Zanuy, M., Mekyska, J., Impedovo, D.: Online handwriting, signature and touch dynamics: tasks and potential applications in the field of security and health. *Cognitive Computation* **13**(5), 1406–1421 (2021) [1](#), [4](#)
10. Fogel, S., Averbuch-Elor, H., Cohen, S., Mazor, S., Litman, R.: Scrabblegan: Semi-supervised varying length handwritten text generation. In: CVPR. pp. 4324–4333 (2020) [4](#)
11. Gan, J., Wang, W.: Higan: handwriting imitation conditioned on arbitrary-length texts and disentangled styles. In: AAAI. vol. 35, pp. 7484–7492 (2021) [4](#), [10](#)
12. Girdhar, R., El-Nouby, A., Liu, Z., Singh, M., Alwala, K.V., Joulin, A., Misra, I.: Imagebind: One embedding space to bind them all. In: CVPR. pp. 15180–15190 (2023) [1](#)
13. Graves, A.: Generating sequences with recurrent neural networks. arXiv preprint arXiv:1308.0850 (2013) [4](#), [5](#)
14. Gutmann, M., Hyvärinen, A.: Noise-contrastive estimation: A new estimation principle for unnormalized statistical models. In: AISTATS. pp. 297–304. JMLR Workshop and Conference Proceedings (2010) [4](#)
15. Hadsell, R., Chopra, S., LeCun, Y.: Dimensionality reduction by learning an invariant mapping. In: CVPR. vol. 2, pp. 1735–1742. IEEE (2006) [4](#)
16. He, K., Zhang, X., Ren, S., Sun, J.: Deep residual learning for image recognition. In: CVPR. pp. 770–778 (2016) [27](#)
17. Jungo, M., Wolf, B., Maksai, A., Musat, C., Fischer, A.: Character queries: a transformer-based approach to on-line handwritten character segmentation. In: ICDAR. pp. 98–114. Springer (2023) [10](#), [25](#)
18. Kang, L., Riba, P., Wang, Y., Rusinol, M., Fornés, A., Villegas, M.: Ganwriting: content-conditioned generation of styled handwritten word images. In: ECCV. pp. 273–289. Springer (2020) [4](#)

19. Khosla, P., Teterwak, P., Wang, C., Sarna, A., Tian, Y., Isola, P., Maschinot, A., Liu, C., Krishnan, D.: Supervised contrastive learning. *NeurIPS* **33**, 18661–18673 (2020) [4](#)
20. Kotani, A., Tellex, S., Tompkin, J.: Generating handwriting via decoupled style descriptors. In: *ECCV*. pp. 764–780. Springer (2020) [2](#), [4](#), [10](#), [14](#), [23](#), [25](#), [32](#), [33](#), [34](#), [35](#)
21. Lee, H., Verma, B.: Over-segmentation and neural binary validation for cursive handwriting recognition. In: *International Joint Conference on Neural Networks (IJCNN)*. pp. 1–5. IEEE (2010) [4](#)
22. Liu, C.L., Yin, F., Wang, D.H., Wang, Q.F.: Casia online and offline chinese handwriting databases. In: *ICDAR*. pp. 37–41. IEEE (2011) [10](#), [25](#)
23. Liu, Y., Khalid, F.B., Wang, L., Zhang, Y., Wang, C.: Elegantly written: Disentangling writer and character styles for enhancing online chinese handwriting. In: *ECCV*. pp. 409–425. Springer (2024) [4](#), [13](#)
24. Liwicki, M., Bunke, H.: Iam-ondb-an on-line english sentence database acquired from handwritten text on a whiteboard. In: *ICDAR*. pp. 956–961. IEEE (2005) [5](#), [10](#), [23](#), [24](#), [25](#)
25. Luo, C., Zhu, Y., Jin, L., Li, Z., Peng, D.: Slogan: handwriting style synthesis for arbitrary-length and out-of-vocabulary text. *TNNLS* **34**(11), 8503–8515 (2022) [4](#)
26. Mitrevski, B., Rak, A., Schnitzler, J., Li, C., Maksai, A., Berent, J., Musat, C.C.: Inksight: Offline-to-online handwriting conversion by teaching vision-language models to read and write. *TMLR* (2025) [4](#)
27. Nakatsuru, K., Uchida, S.: Learning to kern: Set-wise estimation of optimal letter space. In: *ICDAR*. pp. 18–34. Springer (2024) [4](#)
28. Ott, F., Rügamer, D., Heublein, L., Hamann, T., Barth, J., Bischl, B., Mutschler, C.: Benchmarking online sequence-to-sequence and character-based handwriting recognition from imu-enhanced pens. *IJDAR* **25**(4), 385–414 (2022) [1](#), [4](#)
29. Pan, W., He, H., Cheng, H., Shi, Y., Jin, L.: Diffink: Glyph- and style-aware latent diffusion transformer for text to online handwriting generation. In: *ICLR* (2026), <https://openreview.net/forum?id=XKOEQFKFdL> [11](#)
30. Peebles, W., Xie, S.: Scalable diffusion models with transformers. In: *ICCV*. pp. 4195–4205 (2023) [1](#)
31. Plamondon, R., Srihari, S.N.: Online and off-line handwriting recognition: a comprehensive survey. *IEEE TPAMI* **22**(1), 63–84 (2002) [4](#)
32. Ramer, U.: An iterative procedure for the polygonal approximation of plane curves. *Comput. Graph. Image Process.* **1**(3), 244–256 (1972) [11](#), [25](#), [26](#)
33. Ren, M., Zhang, Y.M., Chen, Y.: Decoupling layout from glyph in online chinese handwriting generation. In: *ICLR* (2025), <https://openreview.net/forum?id=DhHIw9Nbl1> [2](#), [4](#), [5](#), [10](#), [14](#), [25](#), [26](#)
34. Su, J., Ahmed, M., Lu, Y., Pan, S., Bo, W., Liu, Y.: Roformer: Enhanced transformer with rotary position embedding. *Neurocomputing* **568**, 127063 (2024) [8](#)
35. Tang, S., Lian, Z.: Write like you: Synthesizing your cursive online chinese handwriting via metric-based meta learning. In: *CGF*. vol. 40, pp. 141–151. Wiley Online Library (2021) [4](#), [13](#)
36. Tang, S., Xia, Z., Lian, Z., Tang, Y., Xiao, J.: Fontrnn: Generating large-scale chinese fonts via recurrent neural network. In: *CGF*. vol. 38, pp. 567–577. Wiley Online Library (2019) [4](#), [5](#)
37. Tolosana, R., Delgado-Santos, P., Perez-Uribe, A., Vera-Rodriguez, R., Fierrez, J., Morales, A.: Deepwritesyn: On-line handwriting synthesis via deep short-term representations. In: *AAAI*. vol. 35, pp. 600–608 (2021) [4](#), [5](#)

38. Vaswani, A., Shazeer, N., Parmar, N., Uszkoreit, J., Jones, L., Gomez, A.N., Kaiser, L., Polosukhin, I.: Attention is all you need. *NeurIPS* **30** (2017) [5](#)
39. Xue, L., Barua, A., Constant, N., Al-Rfou, R., Narang, S., Kale, M., Roberts, A., Raffel, C.: Byt5: Towards a token-free future with pre-trained byte-to-byte models. *TACL* **10**, 291–306 (2022) [4](#), [6](#)
40. Zhang, X.Y., Yin, F., Zhang, Y.M., Liu, C.L., Bengio, Y.: Drawing and recognizing chinese characters with recurrent neural network. *IEEE TPAMI* **40**(4), 849–862 (2017) [4](#), [5](#), [13](#)
41. Zhao, B., Tao, J., Yang, M., Tian, Z., Fan, C., Bai, Y.: Deep imitator: Handwriting calligraphy imitation via deep attention networks. *Pattern Recognition* **104**, 107080 (2020) [4](#), [5](#), [13](#)

# Appendices for CASHG: Context-Aware Stylized Online Handwriting Generation

## A Training Details and Curriculum Schedule

### A.1 Three-Stage Curriculum

Sentence-level online handwriting generation remains challenging under limited compositional diversity because many predecessor–current transitions are under-represented in sentence data. To address this, CASHG adopts a cumulative three-stage curriculum (*glyph*  $\rightarrow$  *bigram*  $\rightarrow$  *sentence*). This design strengthens local boundary modeling before the model is exposed to full sentence composition and helps preserve representative glyph quality throughout training.

Figure A1 summarizes the stage-wise curriculum used in CASHG. Each stage is associated with a different sub-dataset and a different generation target. As the stage increases, the training task expands from representative glyph formation to predecessor–current bigram modeling and then to full sentence generation. Figure A2 further shows that supervision is cumulative rather than replaced across stages.

### A.2 Loss Configuration

At stage  $k$ , the total objective is

$$\mathcal{L}_{\text{total}}^{(k)} = \mathcal{L}_{\text{gen}}^{(k)} + \lambda_{\text{style}}^{(k)} \mathcal{L}_{\text{style}}, \quad (\text{A1})$$

where the active generation loss is

$$\mathcal{L}_{\text{gen}}^{(k)} = \lambda_{\text{char}}^{(k)} \mathcal{L}_{\text{char}} + \lambda_{\text{bi}}^{(k)} \mathcal{L}_{\text{bi}} + \lambda_{\text{sent}}^{(k)} \mathcal{L}_{\text{sent}}. \quad (\text{A2})$$

The three terms correspond to representative glyph samples, predecessor–current bigram windows, and sentence sliding windows, respectively.

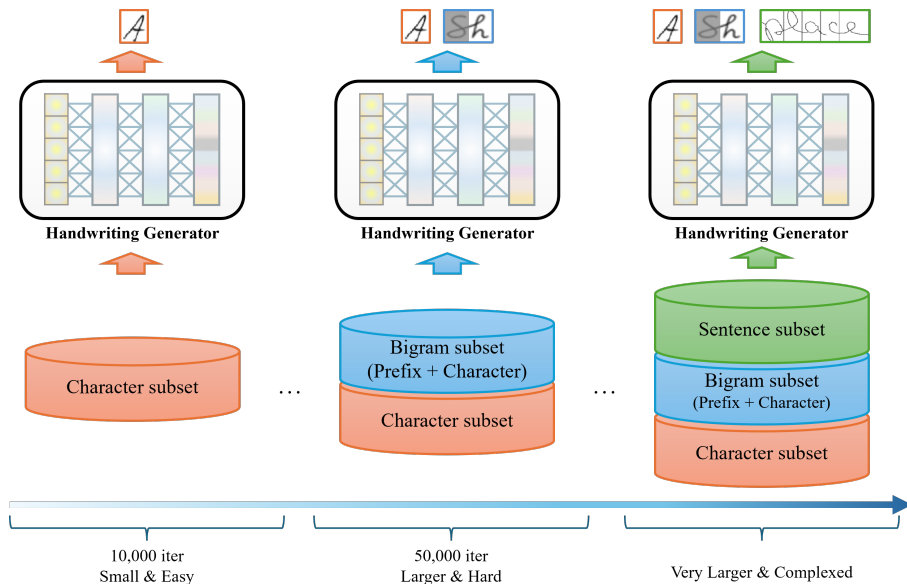
For all active streams, the shared sequence-generation objective is

$$\mathcal{L}_{\text{seq}} = \mathcal{L}_{\text{mdn}} + \lambda_{\text{pen}} \mathcal{L}_{\text{pen}}, \quad (\text{A3})$$

where  $\mathcal{L}_{\text{mdn}}$  is the masked GMM negative log-likelihood on valid trajectory steps and  $\mathcal{L}_{\text{pen}}$  is the masked cross-entropy over the four pen states {PM, PU, CURSIVEEOC, EOC}. In the merged English setting, we use  $\lambda_{\text{pen}} = 1.5$ . The pen-state class weights are [1.0, 1.0, 2.0, 2.5] for [PM, PU, CURSIVE\_EOC, EOC].

For the bigram and sentence streams, we additionally use a Vertical Drift Loss (VDL) term:

$$\mathcal{L}_{\text{bi}} = \mathcal{L}_{\text{seq}} + \lambda_{\text{vdl}}^{\text{bi}} \mathcal{L}_{\text{vdl}}, \quad \mathcal{L}_{\text{sent}} = \mathcal{L}_{\text{seq}} + \lambda_{\text{vdl}}^{\text{sent}}(t) \mathcal{L}_{\text{vdl}}. \quad (\text{A4})$$



**Fig. A1: Stage-wise curriculum and sub-dataset composition in CASHG.** Stage 1 uses the character subset and learns representative glyph generation. Stage 2 adds the bigram subset and learns predecessor–current transitions. Stage 3 further adds the sentence subset and learns sentence-level generation while retaining the earlier streams. In the merged English setting, Stage 1 is used up to 10k iterations, Stage 2 up to 50k iterations, and Stage 3 for the remaining iterations.

The style objective is

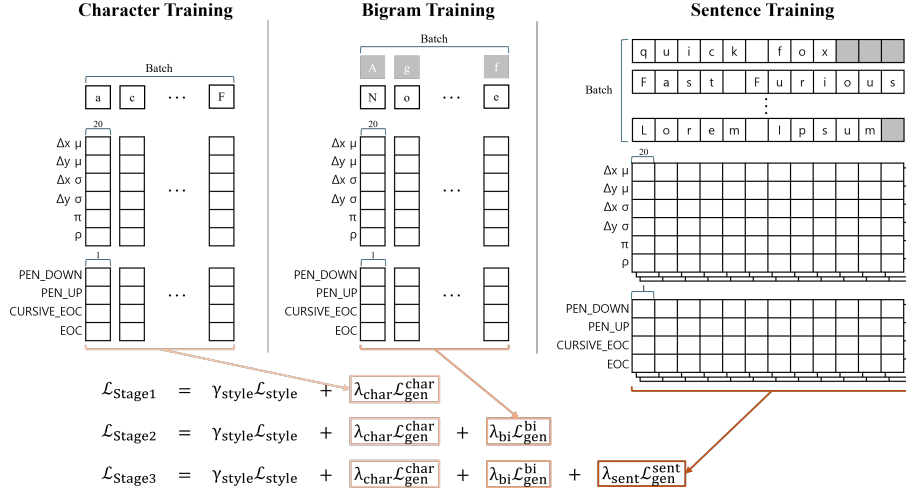
$$\mathcal{L}_{\text{style}} = \mathcal{L}_{\text{SupCon}}^{\text{writer}} + \mathcal{L}_{\text{SupCon}}^{\text{glyph}}. \quad (\text{A5})$$

Table A1 summarizes the main optimization hyperparameters used in the merged English sentence setting. Architecture-specific details such as the context encoder, Bi-SWT decoder, and GMM output head are described separately in Section C.

All experiments in the reported merged English setting were conducted on a single NVIDIA H100 GPU. Under this setup, full training required approximately 10 days.

### A.3 Stage Transition Schedule

In the merged English setting, Stage 1 is used for the first 10k iterations, Stage 2 from 10k to 50k iterations, and Stage 3 for the remaining iterations. The curriculum is cumulative: Stage 1 activates only the character stream, Stage 2 activates both the character and bigram streams, and Stage 3 activates character, bigram, and sentence streams together. Stage transitions use an additional 1k-iteration



**Fig. A2: Cumulative supervision across stages in CASHG.** Stage 1 uses character-level supervision. Stage 2 adds bigram-level supervision together with VDL while retaining the character stream. Stage 3 further adds sentence-level supervision while keeping the earlier streams active.

warmup to reduce instability caused by abrupt changes in the effective data distribution.

Table A2 summarizes the stage-wise curriculum, active coefficients, and nominal minibatch ratios used in the merged English configuration. Stage 2 emphasizes bigram generation while retaining a reduced character stream, and Stage 3 shifts the main emphasis to sentence generation while preserving lower-level supervision. The nominal Stage 3 minibatch ratio is 1 : 1 : 4, reflecting one character batch, one bigram batch, and sentence batches accumulated over four steps.

*Implementation mapping.* In the current merged English configuration, we set the configuration in Stage 1 as below:

- CHAR\_STEP\_STYLE\_LOSS\_WEIGHT=1.0
- CHAR\_STEP\_CHAR\_GEN\_LOSS\_WEIGHT=1.0

In Stage 2, we set the configuration as:

- BIGRAM\_STEP\_STYLE\_LOSS\_WEIGHT=0.3
- BIGRAM\_STEP\_CHAR\_GEN\_LOSS\_WEIGHT=0.3
- BIGRAM\_STEP\_BIGRAM\_GEN\_LOSS\_WEIGHT=1.0

In Stage 3, we set the configuration as:

- STAGE3\_BIGRAM\_STEP\_BIGRAM\_GEN\_LOSS\_WEIGHT=0.5
- SENT\_STEP\_STYLE\_LOSS\_WEIGHT=0.2
- SENT\_STEP\_CHAR\_GEN\_LOSS\_WEIGHT=0.3

**Table A1: Optimization and training hyperparameters used in the merged English sentence setting.**

Field	Setting
Optimizer	AdamW (fused=True)
Base learning rate	8e-5
Max iterations	1,000,000
Initial warmup	30k iterations
Stage-transition warmup	1k iterations
Mixed precision	USE_AMP=false
Gradient clipping	global norm 1.0 for all stages
Batch size	CHAR=64, BIGRAM=64, SENT=16
Gradient accumulation	Stage 1 1, Stage 2 1, Stage 3-char 1, Stage 3-sent 4
Contrastive temperature	Stage 2/3: 0.07

**Table A2: Stage-wise curriculum schedule in the merged English sentence setting.** Later stages retain lower-level streams and add new supervision cumulatively.

Stage	Iterations	$\lambda_{\text{char}}$	$\lambda_{\text{bi}}$	$\lambda_{\text{sent}}$	$\lambda_{\text{style}}$	$\lambda_{\text{vdl}}$	Minibatch ratio
1	[0, 10k)	1	0	0	1.0	0	1:0:0
2	[10k, 50k)	1	1	0	0.3	0.01	1:1:0
3	[50k, 10 <sup>6</sup> ]	1	1	1	0.2	sentence warmup	1:1:4

– STAGE3\_USE\_BIGRAM=true

Accordingly, Stage 1 focuses on representative glyph formation, Stage 2 focuses on predecessor–current boundary modeling, and Stage 3 performs sentence-level generation while retaining lower-level supervision.

#### A.4 Vertical Drift Loss

CASHG predicts trajectories in delta coordinates. This reduces per-step prediction difficulty, but sentence generation remains vulnerable to accumulated predecessor errors, which can induce vertical misalignment across character boundaries. To reduce such drift, we use a lightweight Vertical Drift Loss (VDL) on valid adjacent character boundaries. In the merged English setting, VDL is introduced in Stage 2 through the bigram stream and remains active in Stage 3 through the sentence stream.

Let the predicted delta trajectory be converted to absolute coordinates by cumulative summation. For each character, we extract three vertical summary statistics from the absolute trajectory, namely the *centroid*, *top band*, and *bottom band*. For a valid adjacent boundary  $b = (s - 1, s) \in \mathcal{B}$ , we define the previous-

to-current vertical offsets as

$$\delta_b^{\text{cen}} = \text{cen}(s) - \text{cen}(s-1), \quad (\text{A6})$$

$$\delta_b^{\text{top}} = \text{top}(s) - \text{top}(s-1), \quad (\text{A7})$$

$$\delta_b^{\text{bot}} = \text{bot}(s) - \text{bot}(s-1), \quad (\text{A8})$$

and analogously  $\hat{\delta}_b^{\text{cen}}$ ,  $\hat{\delta}_b^{\text{top}}$ , and  $\hat{\delta}_b^{\text{bot}}$  for the prediction. The VDL objective is then

$$\mathcal{L}_{\text{vdl}} = \frac{1}{|\mathcal{B}|} \sum_{b \in \mathcal{B}} \left( w_{\text{cen}} \|\hat{\delta}_b^{\text{cen}} - \delta_b^{\text{cen}}\|_2^2 + w_{\text{top}} \|\hat{\delta}_b^{\text{top}} - \delta_b^{\text{top}}\|_2^2 + w_{\text{bot}} \|\hat{\delta}_b^{\text{bot}} - \delta_b^{\text{bot}}\|_2^2 \right). \quad (\text{A9})$$

In the current merged English configuration, we use

$$w_{\text{cen}} = 2.0, \quad w_{\text{top}} = 1.0, \quad w_{\text{bot}} = 1.0. \quad (\text{A10})$$

The Stage 2 bigram stream uses a fixed coefficient

$$\lambda_{\text{vdl}}^{\text{bi}} = 0.01, \quad 10\text{k} \leq t < 50\text{k}. \quad (\text{A11})$$

After Stage 3 begins, sentence-level VDL is warmed up separately:

$$\lambda_{\text{vdl}}^{\text{sent}}(t) = \begin{cases} 0, & 50\text{k} \leq t < 60\text{k}, \\ 0.02 \cdot \min\left(1, \frac{t - 60\text{k}}{20\text{k}}\right), & 60\text{k} \leq t < 80\text{k}, \\ 0.02, & t \geq 80\text{k}. \end{cases} \quad (\text{A12})$$

Thus, VDL is active at the bigram level from Stage 2 onward, while the sentence-level VDL term is introduced more conservatively after Stage 3 begins.

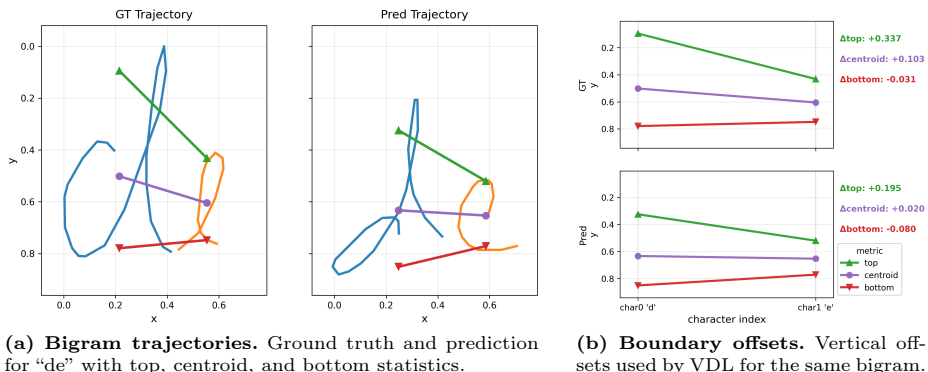
Figure A3 illustrates this computation on the bigram “de”. The left panel shows how the top band, centroid, and bottom band are extracted from the ground-truth and predicted trajectories. The right panel shows the corresponding previous-to-current offsets. By penalizing the discrepancy between these offsets rather than absolute coordinates, VDL directly regularizes relative vertical alignment across adjacent characters.

*Numerical example of VDL.* Figure A3 also provides a concrete example on the bigram boundary  $b = (d, e)$ . In this case,  $|\mathcal{B}| = 1$ . Using the measured values shown in the figure, the ground-truth and predicted vertical offsets are

$$\delta_b^{\text{top}} = 0.336806, \quad \hat{\delta}_b^{\text{top}} = 0.195319, \quad (\text{A13})$$

$$\delta_b^{\text{cen}} = 0.103238, \quad \hat{\delta}_b^{\text{cen}} = 0.019994, \quad (\text{A14})$$

$$\delta_b^{\text{bot}} = -0.031129, \quad \hat{\delta}_b^{\text{bot}} = -0.079883. \quad (\text{A15})$$



**Fig. A3: Illustration of VDL on the bigram “de”.** The left panel shows how top, centroid, and bottom statistics are defined on the ground-truth and predicted trajectories. The right panel shows the corresponding previous-to-current vertical offsets. VDL penalizes the mismatch between these offsets and directly regularizes relative vertical alignment across adjacent characters.

The corresponding squared errors are

$$\ell_{\text{top}} = (\hat{\delta}_b^{\text{top}} - \delta_b^{\text{top}})^2 = 0.020018, \quad (\text{A16})$$

$$\ell_{\text{cen}} = (\hat{\delta}_b^{\text{cen}} - \delta_b^{\text{cen}})^2 = 0.006930, \quad (\text{A17})$$

$$\ell_{\text{bot}} = (\hat{\delta}_b^{\text{bot}} - \delta_b^{\text{bot}})^2 = 0.002377. \quad (\text{A18})$$

Using  $w_{\text{cen}} = 2.0$  and  $w_{\text{top}} = w_{\text{bot}} = 1.0$ , we obtain

$$\mathcal{L}_{\text{vdl}} = \frac{1}{|\mathcal{B}|} \sum_{b \in \mathcal{B}} (1.0 \ell_{\text{top}} + 2.0 \ell_{\text{cen}} + 1.0 \ell_{\text{bot}}) \quad (\text{A19})$$

$$= 1.0(0.020018) + 2.0(0.006930) + 1.0(0.002377) \quad (\text{A20})$$

$$= 0.036255. \quad (\text{A21})$$

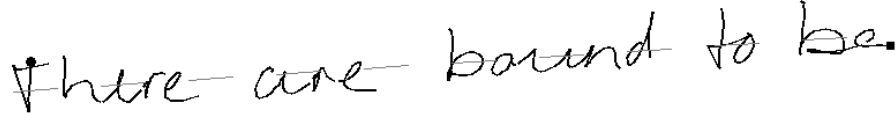
This example shows that VDL is determined by relative boundary-wise vertical mismatch. In practice, this term is active in Stage 2 at the bigram level and is later strengthened in Stage 3 through the sentence-level warmup schedule in Eq. (A12).

## B Dataset Construction and Preprocessing

### B.1 IAM-BRUSH Harmonization

For qualitative examples, human evaluation, and ablation, we construct a merged English sentence dataset from IAM-ONDB [24] and BRUSH [20]. The goal of this merged setting is to increase the diversity of predecessor-current character

BEFORE (angle=-3.74°)



AFTER (deskewed)



**Fig. A4: Sentence-level deskewing on IAM-ONDB [24].** We estimate the global writing angle by least-squares line fitting and rotate the trajectory to reduce sentence-level skew while preserving the original shape.

transitions available to the Bi-SWT decoder. This is particularly useful for modeling boundary-local phenomena such as cursive joins, kerning, and local spacing patterns.

Although both datasets provide online English handwriting trajectories, they differ in coordinate conventions, point-density distributions, and sentence-level geometric bias. A naive merge can therefore introduce domain mismatch, distort trajectory statistics, and destabilize boundary behavior across datasets. To reduce this mismatch, we apply a harmonization pipeline before combining the data.

We observed that IAM-ONDB [24] sentences often exhibit sentence-level skew. For this reason, we apply a lightweight deskewing procedure to IAM samples before merging. Given the sentence trajectory, we fit a line

$$y = mx + b, \quad (\text{A22})$$

by least-squares estimation and compute the sentence angle as

$$\theta = \arctan(m). \quad (\text{A23})$$

The trajectory is then rotated by  $-\theta$  to reduce the estimated sentence-level skew. To avoid unnecessary or unstable correction, we skip deskewing when the estimated angle is either too small to be meaningful or too large to be reliable. Figure A4 shows a representative example. This preprocessing is applied only to the IAM [24] side because BRUSH does not show the same systematic skew pattern in our merged-data preparation.

Because the merged setting is used for connectivity-sensitive sentence generation, we additionally review character segmentation and boundary consistency

on the IAM [24] side. In particular, we follow a segmentation-review procedure inspired by *Character Queries* [17] to identify and correct obvious segmentation inconsistencies before building the merged set. This step is important because boundary-aware supervision in CASHG, including CURSIVEEOC-based connectivity modeling, depends on reliable character boundaries.

The merged English dataset is used for qualitative examples, human evaluation design support, and the ablation setting reported in the paper. Its role is to provide richer local transition coverage for sentence generation. However, this merged setting is not used for benchmark-matched quantitative comparison. For pairwise benchmark comparisons, CASHG is retrained under each benchmark-specific protocol rather than evaluated on the merged set. This keeps the comparisons compatible with the conventions of the corresponding baseline setting.

## B.2 Resampling and RDP Settings

IAM-ONDB [24] and BRUSH [20] differ not only in coordinate convention but also in the number of trajectory points per character. To reduce this mismatch, we primarily use arc-length-based resampling so that the number of points can be adjusted while preserving the overall stroke shape as much as possible. When further reduction is needed, we apply only a weak Ramer–Douglas–Peucker (RDP) [7, 32] simplification.

Figure A5 shows representative examples. We intentionally prefer resampling over aggressive simplification because excessive trajectory reduction can damage local shape cues and degrade boundary realism.

Importantly, the start and end points of every stroke are preserved during preprocessing. This prevents corruption of explicit pen-state events such as PU, EOC, and CURSIVEEOC, which are later used for connectivity-aware supervision and evaluation.

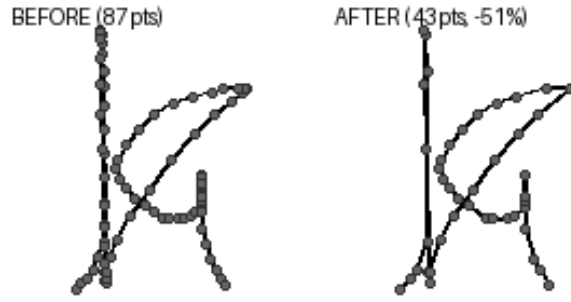
## B.3 Height Normalization

After deskewing and segmentation review, all sentence trajectories are normalized into a shared coordinate system. Following the normalization style adopted in the OLHWG [33]-compatible setting, we normalize each sentence to have height 1.0 while preserving aspect ratio. This harmonizes the overall spatial scale across datasets without distorting writer-specific horizontal spacing patterns.

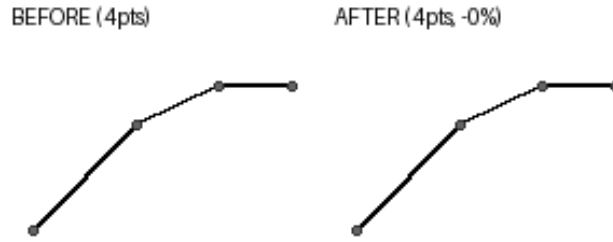
The same normalization principle is also applied to downstream sentence-level preprocessing in order to keep trajectory scale comparable across samples and across datasets. In particular, scale harmonization is performed after geometric cleanup so that skew correction and point-density processing do not interact with inconsistent raw coordinate ranges.

## B.4 Chinese Protocol Details

For the Chinese experiments, we follow the same comparison protocol used in the OLHWG [33] study. Specifically, we use the OLHWD [22] data provided by that



(a) **Resampling with weak RDPRDP** [7, 32]. The number of points is reduced by 51% while the overall trajectory is nearly unchanged.



(b) **Resampling and RDP skipped**. Preprocessing is skipped when the same operation would alter the original shape.

**Fig. A5: Examples of point-density harmonization.** Resampling and weak RDP can substantially reduce the number of points while preserving the original trajectory. When the same preprocessing would distort the shape, both steps are skipped.

study, which is based on CASIA-OLHWDB 2.0–2.2. To keep the comparison aligned with OLHWG the train/test split is defined by writer ID, using writers 0–1019 for training and writers 1020–1218 for evaluation.

To minimize protocol differences other than model architecture, the preprocessing outputs are converted into the unified CASHG sub-dataset format used for training, namely character-level, sentence-level, and style-reference subsets. This allows the Chinese experiments to follow the same training pipeline as the English setting while preserving the writer split and sentence protocol adopted in the OLHWG [33] benchmark.

We apply strict sentence-segmentation validation during preprocessing. If the sum of character durations does not match the total trajectory length, the sentence is discarded. Likewise, if a character boundary implied by the duration annotations does not align with a stroke end marker within a tolerance of  $\pm 3$  points, the sentence is discarded. These checks reduce segmentation noise before boundary-aware training and evaluation.

The coordinate transformation and normalization order is also fixed explicitly. First, the original relative coordinates are converted into absolute coordinates by cumulative summation. Next, deskewing is applied at the sentence level. Finally, the full sentence trajectory is normalized to height 1.0. This ordering stabilizes global sentence geometry before local character windows are extracted.

Long Chinese character trajectories are additionally stabilized by point-count control. When the number of points in a character exceeds a predefined threshold (default: 160), the character trajectory is resampled before being written into the final training subset. This prevents unusually long trajectories from dominating sequence length statistics while preserving the overall stroke structure needed for online handwriting generation.

## C Implementation Details of CASHG

In the reported model, we use `google/canine-c` [5] as the text backbone and a ResNet18 [16]-based style identifier. We choose CANINE primarily for training efficiency while retaining character-level text encoding capability, although the framework is not restricted to CANINE and could be paired with other character-aware text encoders. For style encoding, we adopt ResNet18 by following the stylization strategy of SDT [6], since the style input consists of binary single-channel handwriting images and a lightweight convolutional backbone is more suitable for feature extraction than heavier vision backbones. In our implementation, the CANINE [5] backbone is frozen during training, whereas the ResNet18 [16] style encoder is optimized jointly with the rest of the model.

This section describes the main architectural components of CASHG. Optimization settings, stage-wise schedules, and other training hyperparameters are reported separately in Section A.

### C.1 Character Context Encoder Details

The Character Context Encoder provides two complementary text-side signals for sentence-level generation. It produces a Character-Identity Embedding that specifies which character to draw and a position-dependent Context Memory that modulates how it should appear and connect in sentence context. This role split allows CASHG to preserve character correctness while adapting character realization to local sentence context.

For a Unicode character  $u$ , we encode it in isolation and obtain a deterministic identity embedding

$$\mathbf{e}^{\text{id}}(u) = f_{\text{id}}(f_{\text{text}}([u])) \in \mathbb{R}^D. \quad (\text{A24})$$

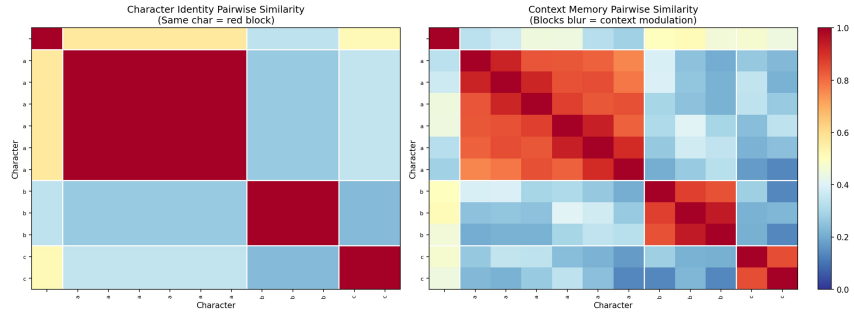
Encoding the character alone avoids contextual leakage and makes the identity pathway act as a stable anchor for content specification. In practice, the identity embedding is cached for unique codepoints within a mini-batch for efficient reuse.

To sharpen discrete identity signals, CASHG uses the augmented identity embedding

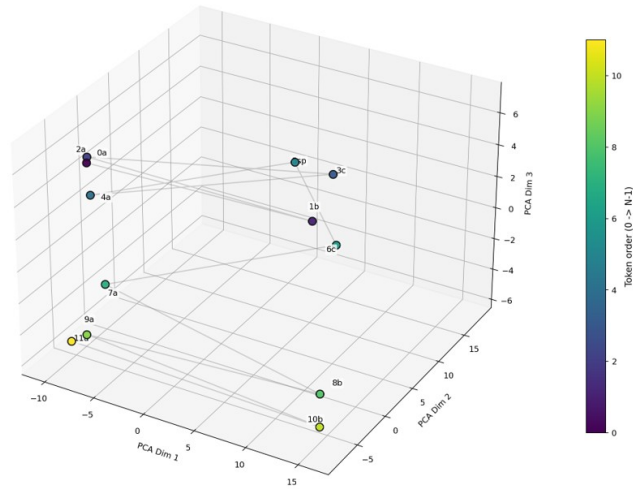
$$\tilde{\mathbf{e}}^{\text{id}}(u) = \mathbf{e}^{\text{id}}(u) + \alpha \mathbf{P}\phi(u), \quad (\text{A25})$$



(a) Single-sentence probe example.



(b) Pairwise similarity of Character-Identity Embedding and Context Memory.



(c) 3D PCA projection of Context Memory tokens.

**Fig. A6: Single-sentence probe of the Character Context Encoder on “abaca cababa”.** (a) Probe sentence example. (b) Pairwise similarity patterns of Character-Identity Embedding and Context Memory. (c) Context Memory tokens projected into a 3D PCA space.

where  $\phi(u)$  is a learnable code embedding,  $\mathbf{P}$  is a projection matrix, and  $\alpha$  is a learnable scalar. This improves identity separability while keeping identity specification separate from sentence-dependent modulation.

For a sentence-level character sequence  $\mathbf{u} = (u_1, \dots, u_S)$ , we compute sentence-aware context features as

$$\mathbf{H}^{\text{text}} = \mathbf{W}_h f_{\text{text}}(\mathbf{u}), \quad \mathbf{M}^{\text{ctx}} = f_{\text{ctx}}(\text{TransEnc}_{\text{ctx}}(\mathbf{H}^{\text{text}})). \quad (\text{A26})$$

The vector  $\mathbf{m}_s^{\text{ctx}}$  varies with neighboring characters and sentence position. This makes it suitable for modeling context-dependent realization and inter-character connectivity such as kerning and cursive joins.

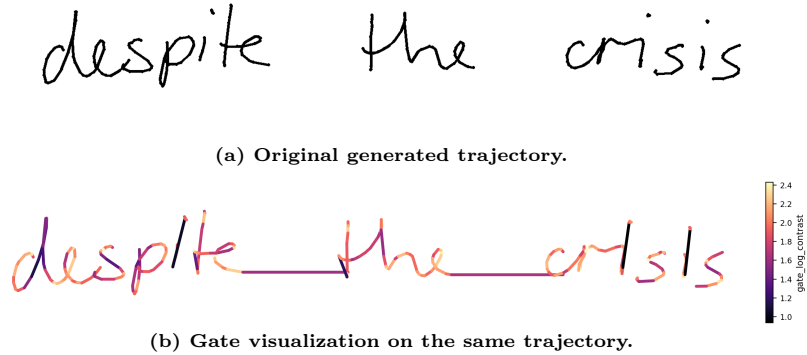
To make this role split concrete, we analyze the two outputs of the Character Context Encoder on a single-sentence probe, “abaca cababa”. This probe contains 12 tokens in total, namely six *a*’s, three *b*’s, two *c*’s, and one space. Figure A6 visualizes the resulting representations. Since the Character-Identity Embedding is computed from isolated-character inputs, it is expected to remain deterministic for each unique codepoint. By contrast, Context Memory is computed from the full sentence and can therefore vary with local position and neighboring characters.

The left panel of Fig. A6 shows a clear difference between the two representations. For the Character-Identity Embedding, same-character pairs form sharp high-similarity blocks, indicating that repeated occurrences of the same character collapse to a stable character-level identity. Quantitatively, the mean same-character similarity is 1.000, whereas the mean different-character similarity is 0.337, yielding a large separation gap of 0.663. By contrast, Context Memory shows visibly blurred same-character blocks. Repeated occurrences of the same character remain related, but no longer collapse to a single invariant template. Here, the mean same-character similarity is 0.857, the mean different-character similarity is 0.298, and the corresponding gap decreases to 0.559. This pattern indicates that the identity branch preserves static character identity, while the context branch retains additional sentence-dependent modulation.

The right panel of Fig. A6 further visualizes Context Memory by a 3D PCA projection. Tokens with different character identities still occupy different regions, but repeated instances of the same character are dispersed rather than collapsed to one point. Moreover, when colored by token order ( $0 \rightarrow N-1$ ), the Context Memory tokens show a gradual movement trend along the sequence. This indicates that the representation carries not only character identity but also context-dependent variation associated with token position and local word structure. Taken together, these observations support the intended role split of the Character Context Encoder: the Character-Identity Embedding specifies *what* to write, while Context Memory modulates *how* it is realized and connected in sentence context.

## C.2 Bigram-Aware Sliding Window Decoder

The handwriting decoder uses a bigram-aware sliding-window design to model predecessor-conditioned local generation. In the reported setting, the decoder operates with hidden dimension 512 and 8 attention heads, and it combines writer-style, glyph-style, and context-conditioned memories through separate decoder



**Fig. A7: Original trajectory and gate visualization.** The top panel shows the generated trajectory. The bottom panel shows the same trajectory colored by log-contrast gate values for gated context fusion. Higher gate responses are more concentrated near cursive connections and boundary regions, indicating stronger use of sentence-dependent context when explicit inter-character continuity is required.

branches. The sliding-window rule is `N_GRAM_AWARE_SLIDING_WINDOW=2`, which corresponds to a bigram prefix.

This design gives the decoder explicit access to the immediately preceding character when generating the current character trajectory. As a result, the model can model local boundary phenomena such as cursive continuation, pen-lift transitions, and boundary-local spacing more reliably than a character-isolated decoder. The predecessor-conditioned window is especially important under sparse sentence-level transition coverage, where many character pairs are not observed frequently enough to be learned robustly from sentence data alone.

During training, the bigram stream is introduced in Stage 2 and retained in Stage 3 together with the sentence stream. This preserves local transition modeling even after full sentence supervision is activated. In this sense, the Bi-SWT decoder and the curriculum design are tightly coupled: the decoder provides an explicit local transition mechanism, while the curriculum ensures that this mechanism is learned before sentence-level composition becomes dominant.

### C.3 Gated Context Fusion

Context memory improves inter-character connectivity, but excessive context injection can interfere with writer style and glyph style. To balance these two effects, CASHG uses a learnable token-wise gated context fusion module. This gate allows local adaptation to sentence context while preserving writer-consistent stylization.

Let  $\mathbf{h}_t^{\text{sty}}$  be the style-conditioned decoder state at token  $t$  and let  $\mathbf{m}_{s(t)}^{\text{ctx}}$  be the context-memory vector associated with the current character position. We compute the gate as

$$\mathbf{g}_t = \sigma \left( f_{\text{gate}} \left( [\mathbf{h}_t^{\text{sty}}; \mathbf{m}_{s(t)}^{\text{ctx}}] \right) \right) \quad (\text{A27})$$

and fuse the two signals as

$$\mathbf{h}_t = (1 - \mathbf{g}_t) \odot \mathbf{h}_t^{\text{sty}} + \mathbf{g}_t \odot \mathbf{m}_{s(t)}^{\text{ctx}}. \quad (\text{A28})$$

Here  $\mathbf{g}_t \in (0, 1)^D$  and  $s(t)$  maps token  $t$  to its character position.

This design gives the decoder two complementary signals. The style pathway provides writer-consistent stylization, while the context pathway provides sentence-dependent modulation related to neighboring characters and position. The gate determines how much context is injected at each token. As a result, CASHG can adapt to local sentence structure without collapsing writer style or glyph style.

The Bi-SWT decoder focuses on predecessor-conditioned local synthesis and handles boundary-local structure through bigram windows. Longer-range sentence information is handled separately through context memory and gated context fusion. The two modules therefore play complementary roles. Bi-SWT captures local transition structure, while gated fusion injects context-dependent modulation on top of that local structure.

Figure A7 shows that the gate response is not uniform along the trajectory. Higher responses are concentrated near character boundaries and cursive-connection regions, whereas many ordinary intra-character stroke regions exhibit lower responses. This spatial pattern indicates that context contribution increases where local realization depends more strongly on neighboring characters.

The same figure also shows that long spacing regions usually have weaker gate responses than boundary-local trajectory segments. In addition, characters whose local form changes little between isolated and sentence contexts often show relatively small gate values. For example, the character  $i$  often changes less across contexts than highly connected cursive characters, and its gate responses are correspondingly weaker. These observations indicate that the gate varies with local context demand rather than remaining constant across the whole sentence.

The sentence-level ablation in the main paper supports this interpretation. Removing gated context fusion preserves part of the DTW [2] benefit but reduces CSM, with the largest drops appearing in  $F1_{\text{cursive}}$  and KGS. This indicates that local bigram modeling alone is not sufficient and that sentence-conditioned context modulation provides an additional benefit for realistic boundary behavior and spacing.

#### C.4 GMM Head Configuration

Trajectory generation is modeled by a Gaussian mixture density head with  $K = 20$  components. For each component, the decoder predicts the parameters

$$(\pi, \mu_x, \mu_y, \sigma_x, \sigma_y, \rho), \quad (\text{A29})$$

where  $\pi$  denotes the mixture weight,  $(\mu_x, \mu_y)$  the mean,  $(\sigma_x, \sigma_y)$  the standard deviations, and  $\rho$  the correlation coefficient. Following stable parameterization practice, we use

$$\sigma = \text{softplus}(\cdot) + \epsilon, \quad \rho = \tanh(\cdot), \quad (\text{A30})$$

with  $\rho$  additionally clamped to  $[-(1 - 10^{-5}), 1 - 10^{-5}]$ . This prevents numerical instability in the bivariate Gaussian covariance near  $|\rho| = 1$ . This output head is shared across curriculum stages and is optimized through the masked GMM negative log-likelihood term defined in Section A.

## D Additional Experimental Analyses

### D.1 Human–Metric Alignment

We further examined whether quantitative metric differences align with human judgments. Because the proposed CSM is a family of four complementary metrics rather than a single scalar, we define an exploratory summary for this analysis:

$$\Delta\text{CSM}_{\text{mean}} = \frac{\Delta\text{F1}_{\text{cursive}} + \Delta\text{CRE} + \Delta\text{KGS} + \Delta\text{SSS}}{4}. \quad (\text{A31})$$

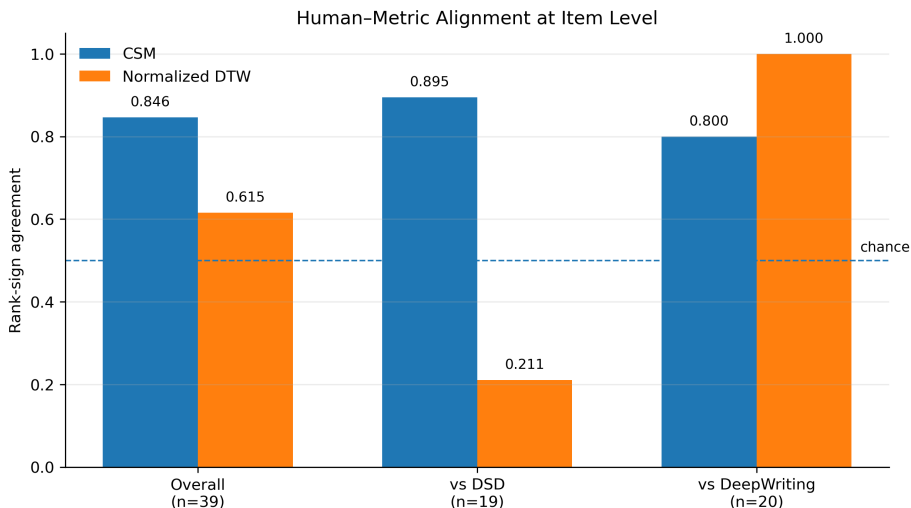
This scalar summary is used only for the alignment analysis and does not replace the separate reporting of the four CSM components in the main evaluation.

Rather than focusing only on continuous correlation strength, we evaluate *rank-sign agreement*, i.e., whether the sign of the metric difference matches the majority human preference direction for each item. Figure A8 compares the resulting agreement rates for  $\Delta\text{CSM}_{\text{mean}}$  and normalized DTW [2] gain.

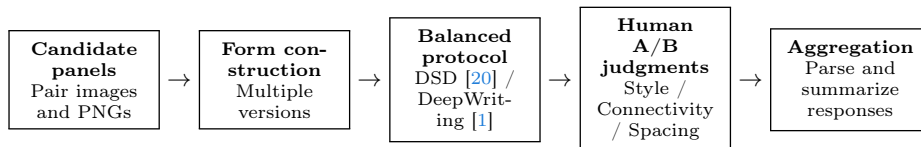
Overall, the mean CSM difference achieves a rank-sign agreement of 0.846, compared with 0.615 for normalized DTW gain. This indicates that, across the full item set, the boundary-aware metric family more often agrees with the direction preferred by human raters.

The protocol-wise behavior is, however, asymmetric. For the DSD [20] comparison, the mean CSM difference reaches 0.895, whereas normalized DTW gain reaches 0.211. This suggests that boundary-aware differences better capture the preferred direction in the DSD setting. By contrast, for the DEEPWRITING [1] comparison, the mean CSM difference reaches 0.800, while normalized DTW gain reaches 1.000. Thus, in the DEEPWRITING setting, the preferred direction is more consistently aligned with normalized DTW gain than with the mean CSM summary.

Taken together, these observations suggest that human–metric alignment is protocol-dependent. The proposed CSM family is more informative for the DSD [20] comparison, where boundary connectivity and spacing appear to be more decisive for human preference, whereas the DEEPWRITING comparison is more consistently aligned with global trajectory similarity as measured by normalized DTW [2]. This analysis therefore supports the view that CSM and DTW provide complementary signals rather than interchangeable ones.



**Fig. A8: Item-level rank-sign agreement between human preference and metric differences.** For each item, we compare the majority human preference with the sign of the metric difference between CASHG and the baseline. For the CSM side, we use an exploratory *mean CSM difference*, defined as the arithmetic mean of  $\Delta F1_{\text{cursive}}$ ,  $\Delta \text{CRE}$ ,  $\Delta \text{KGS}$ , and  $\Delta \text{SSS}$ . Higher values indicate that the metric more often agrees with the human-preferred direction.



**Fig. A9: Human evaluation workflow.** Candidate comparison panels were organized into balanced questionnaire versions, judged on three criteria, and then parsed into criterion-level decisions for aggregation. Numerical details are summarized in Table A3.

## E Human Evaluation Protocol

### E.1 Experimental Design

To complement the quantitative evaluation, we conducted a human A/B study comparing CASHG against DEEPWRITING [1] and DSD [20] in terms of style fidelity, inter-character connectivity, and spacing. The overall procedure is summarized in Fig. A9.

We prepared five questionnaire versions (V1–V5), each containing 20 comparison items. Protocol assignment was balanced within each version: 10 items compared CASHG against DSD [20], and the other 10 compared CASHG against DEEPWRITING [1]. Each item was judged on three criteria—Style, Connectiv-

ity, and Spacing—so that one completed submission produced 60 criterion-level decisions.

Each question consists of three real reference images written by the same writer and two generated candidates for the same target sentence. The two candidates correspond to CASHG and one baseline model, and are shown as Candidate A and Candidate B with randomized left/right assignment to reduce positional bias. The reference images are sampled from three different sentences written by the same writer. Across the full study, the question pool covers 40 sentence IDs, corresponding to 23 unique sentence texts. Measured over unique sentence texts, the character-length statistics are 12 / 16 / 16.18 / 19 for min / median / mean / max, respectively. This range provides enough boundary structure for evaluating connectivity and spacing while keeping the questionnaire manageable for human raters.

All online trajectories are rendered as raster images in PNG format for presentation. For fair visual comparison, the three reference images and the two generated candidates are scaled to the same height. This normalization keeps the comparison focused on writer style, boundary connectivity, and spacing patterns rather than trivial differences in absolute image scale.

In total, we collected 30 submissions, corresponding to six submissions per questionnaire version. Since each submission contains 20 items and each item is judged on three criteria, the study produced 1,800 criterion-level decisions. Among them, 1,604 were valid preference decisions and 196 were marked as *Cannot judge*, corresponding to an abstention rate of 10.9%. Multiple questionnaire versions serve two purposes. They distribute the item pool across raters while keeping the per-rater burden moderate, and they maintain protocol balance between CASHG vs. DSD [20] and CASHG vs. DEEPWRITING [1].

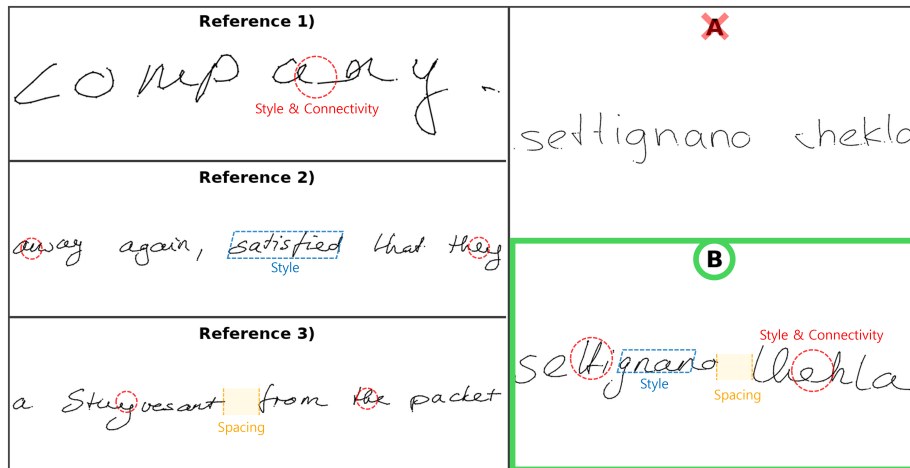
Participants were Korean adults and included a mixed group of graduate students and working professionals. Gender was not controlled and was naturally mixed across participants. Participants were asked to choose which candidate better matched the reference writer under three criteria. **Style** evaluates overall handwriting appearance, including slant, visual tone, rounded versus angular shape, and writing rhythm. **Connectivity** evaluates inter-character connection patterns, including natural continuation or separation between characters and smooth boundary transitions. **Spacing** evaluates spacing between words, including inter-word distance, spacing consistency, and whether gaps appear excessively narrow or wide.

## E.2 Interface Example

To help participants understand the task, the questionnaire begins with the illustrated example in Fig. A10. The example presents three real reference samples from the same writer on the left and two generated candidates on the right. Visual annotations are added only in this example to highlight representative cues for style, connectivity, and spacing, and to clarify the intended interpretation of the three criteria.

**Table A3: Summary of the human evaluation setup and collected responses.**

Item	Value
Questionnaire versions	5 (V1–V5)
Submissions	30 total (6 per version)
Items per version	20 A/B comparison items
Criteria per item	Style / Connectivity / Spacing
Protocol balance	10 DSD [20] + 10 DeepWriting [1] per version
Decisions per submission	60 (= 20 items × 3 criteria)
Total decisions	1,800
Valid / Cannot judge	1,604 / 196
Cannot judge rate	10.9%
Sentence IDs used	40
Unique sentence texts	23
Sentence length over unique texts	min / median / mean / max = 12 / 16 / 16.18 / 19



**Fig. A10: Instruction example shown to participants in the human evaluation.** The left panel shows three real reference samples written by the same writer. The right panel shows two generated candidates for the same target sentence, where one is produced by CASHG and the other by the baseline model. The assignment of CASHG and the baseline to Candidate A and Candidate B is randomized. Colored annotations are included only in this instruction example to illustrate the three evaluation criteria.

Figure A11 shows an example of the actual questionnaire interface used during evaluation. In contrast to the annotated instruction example, the real interface does not provide explanatory highlights. Instead, participants view the reference samples and the two candidates in a neutral layout and record their judgments separately for Style, Connectivity, and Spacing, with an additional

Item 01: "drawcansir holroyd" — Question \*

- Style: letterform vibe (round vs. angular), writing rhythm
- Connectivity: continuity/breaks, boundary transitions, cursive joins
- Spacing: inter-word distance/consistency (relative to text height)

	A	B	Cannot judge
Style	<input type="radio"/>	<input type="radio"/>	<input type="radio"/>
Connectivity	<input type="radio"/>	<input type="radio"/>	<input type="radio"/>
Spacing	<input type="radio"/>	<input type="radio"/>	<input type="radio"/>

---

Item 02: "esquimau frugality" — Option

<p style="text-align: center; font-weight: bold; font-size: small;">Reference 1)</p> <p style="font-family: cursive; font-size: small;">Showing their knowledge. Maybe</p>	<p style="text-align: center; font-weight: bold; font-size: small;">A</p> <p style="font-family: cursive; font-size: small;">esquimau frugality</p>
<p style="text-align: center; font-weight: bold; font-size: small;">Reference 2)</p> <p style="font-family: cursive; font-size: small;">in the hierarchy of their classification</p>	<p style="text-align: center; font-weight: bold; font-size: small;">B</p> <p style="font-family: cursive; font-size: small;">.esquimau frugality</p>
<p style="text-align: center; font-weight: bold; font-size: small;">Reference 3)</p> <p style="font-family: cursive; font-size: small;">Heart. All who were over Jerusalem</p>	

**Fig. A11: Example of the actual questionnaire interface used in the human study.** Each item asks participants to compare Candidate A and Candidate B against three reference samples under three criteria: Style, Connectivity, and Spacing.

*Cannot judge* option. This design helps reduce instructional bias during the actual response stage while preserving criterion-level evaluation.

The annotations are therefore shown only on the instruction page and are not included in the actual evaluation items. This separation ensures that participants receive guidance on the intended criteria before the study begins, while the final judgments themselves are collected from an unannotated interface.

## F Connectivity and Spacing Metrics (CSM)

### F.1 Boundary Formalization

CASHG predicts four pen states at each time step, with the label set {PM, PU, CURSIVEEOC, EOC}. Here CURSIVEEOC denotes an end-of-character event with the pen still down, i.e., an explicit cursive-like continuation to the next character. We use small caps (e.g., CURSIVEEOC) for pen-state labels to avoid code-style font rendering.

Some baseline methods do not predict an explicit CURSIVEEOC label at character boundaries. For such methods, we first mark every character boundary as EOC and then convert EOC  $\rightarrow$  CURSIVEEOC using a distance-based heuristic. Let  $\mathbf{p}_s^{\text{end}}$  be the last point of character  $s$  and let  $\mathbf{p}_{s+1}^{\text{PM}}$  be the first pen-move point of the next character  $s + 1$ . We define the boundary distance

$$d_s^{\text{conn}} = \|\mathbf{p}_s^{\text{end}} - \mathbf{p}_{s+1}^{\text{PM}}\|_2. \quad (\text{A32})$$

On normalized coordinates, we relabel the boundary as CURSIVEEOC when

$$d_s^{\text{conn}} < \tau_{\text{conn}}, \quad \tau_{\text{conn}} = 0.005, \quad (\text{A33})$$

and keep it as EOC otherwise. This heuristic is used only for baselines that do not provide explicit cursive-boundary labels. By contrast, CASHG directly predicts CURSIVEEOC as part of its pen-state output.

Let  $\mathcal{W}$  be the set of writers and  $\mathcal{D}_w$  the set of test sentences for writer  $w \in \mathcal{W}$ . A sentence  $i \in \mathcal{D}_w$  consists of a character sequence  $\mathbf{x}^{(i)} = (x_1^{(i)}, \dots, x_{S_i}^{(i)})$  including spaces, and per-character trajectories  $\mathbf{Y}_s^{(i)} = \{(x_{s,t}, y_{s,t})\}_{t=1}^{T_s^{(i)}}$ . We use the *last* step of each character  $s$  to define a boundary label  $q_s^{(i)} \in \{\text{PM}, \text{PU}, \text{CURSIVEEOC}, \text{EOC}\}$  for the ground truth and  $\hat{q}_s^{(i)}$  for the prediction. We use  $\epsilon > 0$  (e.g.,  $10^{-6}$ ) for numerical stability.

We evaluate inter-character phenomena on *adjacent non-space boundaries*:

$$\mathcal{B}_i = \{s \mid 1 \leq s \leq S_i - 1, x_s^{(i)} \neq \text{space}, x_{s+1}^{(i)} \neq \text{space}\}. \quad (\text{A34})$$

For word spacing, we evaluate *space-run boundaries*:

$$\mathcal{P}_i = \left\{ (u, v) \mid \begin{array}{l} 1 \leq u < v \leq S_i, x_u^{(i)} \neq \text{space}, x_v^{(i)} \neq \text{space}, \\ x_{u+1}^{(i)} = \dots = x_{v-1}^{(i)} = \text{space} \end{array} \right\}. \quad (\text{A35})$$

That is, a run of one or more spaces between two non-space characters is counted once.

We define per-character horizontal bounds from trajectories:

$$L_s^{(i)} = \min_t x_{s,t}^{(i)}, \quad R_s^{(i)} = \max_t x_{s,t}^{(i)}, \quad (\text{A36})$$

and similarly  $\hat{L}_s^{(i)}, \hat{R}_s^{(i)}$  from predicted trajectories.

## F.2 Cursive Metrics (F1cursive, CRE)

We treat CURSIVEEOC as the positive class on eligible boundaries. For CASHG,  $\hat{q}_s^{(i)}$  is read directly from the predicted pen state. For baselines without an explicit CURSIVEEOC label,  $\hat{q}_s^{(i)}$  is obtained by the boundary-conversion heuristic described above. For each boundary  $s \in \mathcal{B}_i$ , we define

$$z_s^{(i)} = \mathbb{I}[q_s^{(i)} = \text{CURSIVEEOC}], \quad \hat{z}_s^{(i)} = \mathbb{I}[\hat{q}_s^{(i)} = \text{CURSIVEEOC}]. \quad (\text{A37})$$

Since F1 is non-linear, we compute  $\text{F1}_{\text{cursive}}$  from writer-level counts rather than averaging per-sentence F1:

$$\text{TP}_w = \sum_{i \in \mathcal{D}_w} \sum_{s \in \mathcal{B}_i} \mathbb{I}[\hat{z}_s^{(i)} = 1 \wedge z_s^{(i)} = 1], \quad (\text{A38})$$

$$\text{FP}_w = \sum_{i \in \mathcal{D}_w} \sum_{s \in \mathcal{B}_i} \mathbb{I}[\hat{z}_s^{(i)} = 1 \wedge z_s^{(i)} = 0], \quad (\text{A39})$$

$$\text{FN}_w = \sum_{i \in \mathcal{D}_w} \sum_{s \in \mathcal{B}_i} \mathbb{I}[\hat{z}_s^{(i)} = 0 \wedge z_s^{(i)} = 1]. \quad (\text{A40})$$

Precision, recall, and F1 are then defined as

$$\text{Prec}_w = \frac{\text{TP}_w}{\text{TP}_w + \text{FP}_w + \epsilon}, \quad \text{Rec}_w = \frac{\text{TP}_w}{\text{TP}_w + \text{FN}_w + \epsilon}, \quad (\text{A41})$$

$$\text{F1}_w^{\text{cursive}} = \frac{2 \text{Prec}_w \text{Rec}_w}{\text{Prec}_w + \text{Rec}_w + \epsilon}. \quad (\text{A42})$$

If  $\sum z_s^{(i)} = 0$  and  $\sum \hat{z}_s^{(i)} = 0$ , we set  $\text{F1}_w^{\text{cursive}} = 1$  by convention.

$\text{F1}_{\text{cursive}}$  measures boundary-level correctness, but writers also differ in how often they use cursive connections. We therefore measure how well the *cursive rate* is matched *per sentence*, which avoids overweighting long sentences. For each sentence  $i$ , we define

$$r_i = \frac{1}{|\mathcal{B}_i| + \epsilon} \sum_{s \in \mathcal{B}_i} z_s^{(i)}, \quad \hat{r}_i = \frac{1}{|\mathcal{B}_i| + \epsilon} \sum_{s \in \mathcal{B}_i} \hat{z}_s^{(i)}. \quad (\text{A43})$$

Sentences with  $|\mathcal{B}_i| = 0$  are still included, yielding  $r_i \approx 0$ . CRE therefore remains well-defined for short or space-heavy sentences. The writer-level mean absolute error is

$$\text{MAE}_w^{\text{rate}} = \frac{1}{|\mathcal{D}_w|} \sum_{i \in \mathcal{D}_w} |\hat{r}_i - r_i|, \quad (\text{A44})$$

and the final similarity score is

$$\text{CRE}_w = \max(0, 1 - \text{MAE}_w^{\text{rate}}). \quad (\text{A45})$$

### F.3 Spacing Metrics (KGS, SSS)

For adjacent non-space characters, we define the kerning gap on boundary  $s \in \mathcal{B}_i$  as

$$g_s^{(i)} = L_{s+1}^{(i)} - R_s^{(i)}, \quad \hat{g}_s^{(i)} = \hat{L}_{s+1}^{(i)} - \hat{R}_s^{(i)}. \quad (\text{A46})$$

Since gaps can be negative when characters overlap, we use a non-negative gap  $g^+ = \max(g, 0)$  and apply an overlap penalty to avoid assigning a perfect score when both are heavily overlapping. Let  $\rho \in (0, 1]$  and we use  $\rho = 0.5$ :

$$\pi(g, \hat{g}) = \rho^{\mathbb{I}[g < 0 \vee \hat{g} < 0]}. \quad (\text{A47})$$

We then use a symmetric log-ratio similarity:

$$\text{KGS}_s^{(i)} = \pi\left(g_s^{(i)}, \hat{g}_s^{(i)}\right) \cdot \exp\left(-\left|\log \frac{\max(\hat{g}_s^{(i)}, 0) + \epsilon}{\max(g_s^{(i)}, 0) + \epsilon}\right|\right). \quad (\text{A48})$$

For each word-gap boundary  $(u, v) \in \mathcal{P}_i$ , we define the word spacing width as

$$d_{u \rightarrow v}^{(i)} = L_v^{(i)} - R_u^{(i)}, \quad \hat{d}_{u \rightarrow v}^{(i)} = \hat{L}_v^{(i)} - \hat{R}_u^{(i)}. \quad (\text{A49})$$

We use the same log-ratio similarity with the same overlap handling:

$$\text{SSS}_{u \rightarrow v}^{(i)} = \pi\left(d_{u \rightarrow v}^{(i)}, \hat{d}_{u \rightarrow v}^{(i)}\right) \cdot \exp\left(-\left|\log \frac{\max(\hat{d}_{u \rightarrow v}^{(i)}, 0) + \epsilon}{\max(d_{u \rightarrow v}^{(i)}, 0) + \epsilon}\right|\right). \quad (\text{A50})$$

Thus, KGS evaluates spacing similarity on adjacent non-space character boundaries, while SSS evaluates spacing similarity across word gaps containing one or more spaces. Both metrics are geometry-based and remain directly comparable even when cursive boundary labels for baselines are inferred heuristically.

#### F.4 Writer-Macro Aggregation

For spacing metrics, writer-level aggregation is computed by averaging over eligible boundaries. For KGS, we use

$$\text{KGS}_w = \frac{\sum_{i \in \mathcal{D}_w} \sum_{s \in \mathcal{B}_i} \text{KGS}_s^{(i)}}{\sum_{i \in \mathcal{D}_w} |\mathcal{B}_i| + \epsilon}, \quad (\text{A51})$$

and for SSS,

$$\text{SSS}_w = \frac{\sum_{i \in \mathcal{D}_w} \sum_{(u,v) \in \mathcal{P}_i} \text{SSS}_{u \rightarrow v}^{(i)}}{\sum_{i \in \mathcal{D}_w} |\mathcal{P}_i| + \epsilon}. \quad (\text{A52})$$

In the paper, we report  $\text{F1}_{\text{cursive}}$ , CRE, KGS, and SSS separately with writer-macro averaging. For the cursive-related metrics, baseline predictions without explicit CURSIVEEOC labels are converted from boundary EOC labels using the distance-based heuristic above. By contrast, KGS and SSS are computed directly from trajectory geometry through horizontal gap measurements. Together, these metrics separate boundary connectivity, local kerning, and inter-word spacing, which are not fully resolved by DTW [2] alone.

Figure A12 provides one concrete example for each CSM component. Panel (a) illustrates  $\text{F1}_{\text{cursive}}$ , where CURSIVEEOC is treated as the positive class and EOC as the negative class on eligible adjacent-character boundaries. This metric evaluates boundary-level correctness through writer-level counts of true positives, false positives, and false negatives.

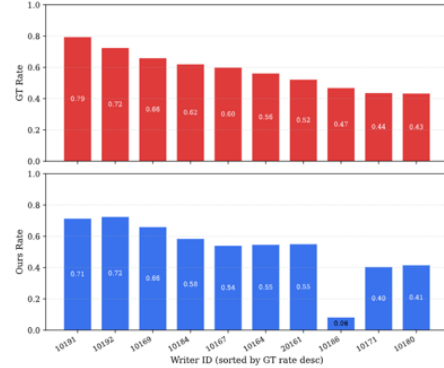
Panel (b) illustrates CRE from writer-level cursive rates. For each writer, we compare the GT cursive rate and the predicted cursive rate and compute the

		Prediction		
		Positive (CURSIVE_EOC)	Negative (EOC)	
Actual (GT)	Positive (EOC_CURSIVE)	<b>TP</b>	<b>FN</b>	<b>Recall</b> $= TP / (TP + FN)$
	Negative (EOC)	<b>FP</b>	<b>TN</b>	

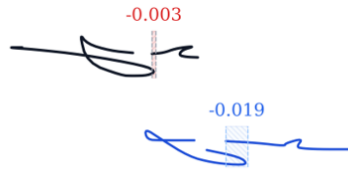
**Precision**  
 $= TP / (TP + FP)$

**F1**  
 $= 2 (P \times R) / (P + R)$

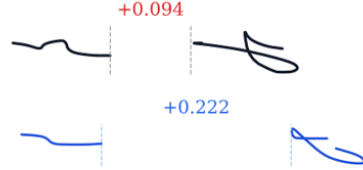
(a) **F1<sub>cursive</sub> example.** Boundary-level confusion matrix for CURSIVEEOC (positive) vs. EOC (negative).



(b) **CRE example.** Writer-level GT and predicted cursive rates on an illustrative set of 10 writers.



(c) **KGS example.** Overlapping adjacent-character gaps receive an overlap penalty.



(d) **SSS example.** Word-gap similarity is measured from the spacing between non-space neighbors.

**Fig. A12: Illustrative examples of the four Connectivity and Spacing Metrics (CSM).** (a)  $F1_{cursive}$  evaluates whether a boundary is correctly classified as cursive-connected (CURSIVEEOC) or non-cursive (EOC). (b) CRE evaluates how well the writer-level cursive usage rate is matched. (c) KGS measures similarity of adjacent-character kerning gaps with overlap-aware penalization. (d) SSS measures similarity of inter-word spacing widths using the same log-ratio form.


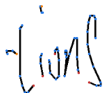


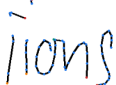




mean absolute difference. In the shown 10-writer example, the average absolute difference is 0.0656, yielding

$$CRE = 1 - 0.0656 = 0.9344. \quad (A53)$$

This example highlights that CRE measures writer-level agreement in *how often* cursive boundaries are used rather than exact boundary-by-boundary matches.

Panels (c) and (d) illustrate KGS and SSS, respectively. Both metrics follow the same overlap-aware log-ratio similarity defined in Eqs. (A48) and (A50). For KGS,  $x$  and  $\hat{x}$  correspond to adjacent-character kerning gaps. For SSS, they correspond to inter-word spacing widths. As shown in panel (c), when both the GT and prediction overlap ( $g_{GT} < 0$  and  $\hat{g} < 0$ ), the overlap penalty is activated and the score becomes

$$KGS = 0.5. \quad (A54)$$

	(a)	(b)	(c)
GT			
Deep Writing [1]			
CASHG			
DTW [2]	DeepWriting: 0.153 CASHG: 0.171	DeepWriting: 0.182 CASHG: 0.186	DeepWriting: 0.437 CASHG: 0.513
CSM mean	DeepWriting: 0.300 CASHG: 0.722	DeepWriting: 0.339 CASHG: 0.714	DeepWriting: 0.352 CASHG: 0.472

**Fig. A13: Representative cases where CSM complements DTW [2].** Panels (a), (b), and (c) show examples in which the DTW values of DEEPWRITING [1] and CASHG are relatively close, while CSM provides clearer discrimination. GT denotes ground truth. The bottom rows report DTW and the arithmetic mean of the four CSM components used in the case-analysis CSV.

In panel (d), the GT and predicted word-gap widths are 0.094 and 0.222, respectively, which gives

$$SSS = \exp\left(-\left|\log \frac{0.222 + \epsilon}{0.094 + \epsilon}\right|\right) \approx 0.4234. \quad (\text{A55})$$

Together, these examples show that the four CSM components capture complementary aspects of boundary connectivity and spacing.

Figure A13 presents representative cases where DTW [2] alone provides only weak separation between competing predictions. In these examples, DEEPWRITING [1] attains slightly lower DTW values than CASHG, yet CASHG shows stronger agreement with boundary-sensitive CSM.

In panel (a), DEEPWRITING obtains a lower DTW [2] than CASHG (0.153 vs. 0.171). However, CASHG achieves substantially higher  $F1_{\text{cursive}}$  (0.714 vs. 0.000), CRE (1.000 vs. 0.364), KGS (0.503 vs. 0.348), and SSS (0.671 vs. 0.488), yielding a much higher CSM mean (0.722 vs. 0.300).

In panel (b), the DTW values are again close (0.182 vs. 0.186), while CASHG shows clear advantages in  $F1_{\text{cursive}}$  (1.000 vs. 0.000), CRE (1.000 vs. 0.750), and KGS (0.856 vs. 0.606). Following the case-analysis CSV, SSS is reported as 0.000

for both methods in this example, giving CSM mean values of 0.714 for CASHG and 0.339 for DEEPWRITING.

In panel (c), DEEPWRITING again attains a lower DTW (0.437 vs. 0.513), but CASHG better matches the ground-truth spacing pattern, reflected by higher KGS (0.437 vs. 0.335) and SSS (0.701 vs. 0.323), while  $F1_{\text{cursive}}$  and CRE are tied at 0.000 and 0.750, respectively. As a result, CASHG also shows a higher CSM mean (0.472 vs. 0.352).

These examples show that CSM complements DTW by explicitly evaluating connectivity and spacing, which are not always sufficiently captured by DTW alone.